VILNIUS UNIVERSITY
CENTER FOR PHYSICAL SCIENCES AND TECHNOLOGY

EGIDIJUS KAMARAUSKAS

INVESTIGATION OF CARBAZOLE- AND HYDRAZONE-BASED CHARGE CARRIER MATERIALS AND DYES FOR SOLAR CELLS

Summary of doctoral dissertation
Technological science
Materials engineering (08T)

Vilnius
2017

Dissertation was prepared in 2010 - 2016 at Vilnius University

Scientific supervisor:

doc. Vygintas Jankauskas (Vilnius university , Technology sciences, materials engineering - 08T)

Scientific consultant:

hab. dr. Valentas Gaidelis (Vilnius university , Technology sciences, materials engineering - 08T)

Dissertation will be defended in Dissertation Defense Board:

Chairman – prof. dr. Roland Tomašiūnas (Center for physical sciences and technology, Technology sciences, materials engineering - 08T).

Members:

prof. habil. dr. Vidmantas Gulbinas (Center for physical sciences and technology, Technology sciences, materials engineering - 08T);

prof. dr. Mihaela Girtan (University of Angers, France, Technology sciences, materials engineering - 08T)

prof. dr. Nerija Žurauskienė (Center for physical sciences and technology, Technology sciences, materials engineering - 08T)

prof. habil. dr. Sigitas Tamulevičius (Kaunas university of technology, Technology sciences, materials engineering - 08T)

Dissertation will be defended under open consideration in council of Dissertation Defense Board on 30rd of October, 3 p. m. at the Center for physical sciences and technology, in B336 room. Address: Saulėtekio al. 3, Vilnius, Lithuania.

The summary of doctoral thesis will be sent on 30th of September, 2017.

The doctoral thesis is available at Vilnius University Library and at the official Vilnius University website:

http://www.vu.lt/lt/naujienos/ivykiu-kalendorius

VILNIAUS UNIVERSITETAS
FIZINIŲ IR TECHNOLOGIJOS MOKSLŲ CENTRAS

EGIDIJUS KAMARAUSKAS

HIDRAZONO BEI KARBAZOLO KRŪVIO PERNAŠOS DARINIŲ BEI DAŽIKLIŲ SAULĖS ELEMENTAMS TYRIMAI

Daktaro disertacijos santrauka
Technologijos mokslai
Medžiagų inžinerija (08T)

Vilnius
2017

Disertacija rengta 2010 - 2016 metais Vilniaus universitete.

Mokslinis vadovas:

doc. dr. Vygintas Jankauskas (Vilniaus universitetas, technologijos mokslai, medžiagų inžinerija - 08T)

Mokslinis konsultantas:

habil. dr. Valentas Gaidelis (Vilniaus universitetas, technologijos mokslai, medžiagų inžinerija - 08T)

Disertacija ginama viešame disertacijos Gynimo tarybos posėdyje:

Pirmininkas – prof. dr. Roland Tomašiūnas (Vilniaus universitetas, technologijos mokslai, medžiagų inžinerija - 08T).

Nariai:

prof. habil. dr. Vidmantas Gulbinas (Fizinių ir technologijos mokslų centras, technologijos mokslai, medžiagų inžinerija - 08T);

prof. dr. Mihaela Girtan (Angers universitetas, Prancūzija, technologijos mokslai, medžiagų inžinerija - 08T)

prof. dr. Nerija Žurauskienė (Fizinių ir technologijos mokslų centras, technologijos mokslai, medžiagų inžinerija - 08T)

prof. habil. dr. Sigitas Tamulevičius (Kauno technologijos universitetas, technologijos mokslai, medžiagų inžinerija - 08T)

Disertacija bus ginama viešame disertacijos Gynimo tarybos posėdyje 2017 m. spalio mėn. 30 d. 15:00 val. Nacionalinio fizinių ir technologijos mokslų centre, B336 auditorijoje. Adresas: Saulėtekio al. 3, Vilnius, Lietuva.

Disertacijos santrauka išsiuntinėta 2017. m. rugsėjo mėn. 30 d.

Disertaciją galima peržiūrėti Vilniaus universiteto bibliotekoje ir VU interneto svetainėje adresu:

http://www.vu.lt/lt/naujienos/ivykiu-kalendorius

Contents

1. Introduction

1.1. Motivation

Nowadays, when air pollution and increased CO_2 levels keeps us anxious, the alternative energy sources became the main interest of society. There are more than a few of these sources as hydro-energy, biomass, wind or photo-voltaic. The latter changes solar light into electric energy directly, also having a high energy potential. For this reason photo-voltaic energy sources attracted main attention and a lot of scientific researches took part on it.

The most popular Solar cells are based on silicon - about 90 percent of market share. However, very pure silicon is needed and the technological process requires part of this energy itself. These SC uses about 1000 times more light absorber then dye-sensitized or perovskite SC, also they are quite thick for negligible light absorption and for high fragility they need a protective layer of glass. As a result, all the construction becomes massive, expensive, therefore useful just in large commercial objects, not for individual home use.

Quite the reverse are dye sensitized SC. They are thin, light, less energy needed into technical process, what results in availability for individual home use. On the other hand, the energy efficiency is slightly lower than silicon SC, but still other mentioned characteristics and price are promising in individual use.

The main issue in DSSC is cheaper and easier to synthesized dye materials and charge transporting materials.

1.2. The structure of dissertation.

The dissertation made of six main parts - introduction, literature review, methods, results, conclusion and literature list.

1.3. Purpose and tasks.

Purpose - find out how organic dyes energetic levels depends on molecular structure and how these levels effects SC characteristics, also explore how potential charge transporting materials holes drift mobility and ionization potencial Ip depends on attached functional groups, using it in SC.

For this reason these tasks were formed:

- Measure the ionization potentials and light absorption spectrum in pure dyes layers, also in dyes, adsorbed on TiO_2;
- Find out dye energetic levels and compare with data from the cyclic voltampermetry measurements and light absoption spectrum in dye solutions;
- Measure the ionization potentials and holes drift mobility in holes transporting materials.
- Make dye sensitized SC with the most suitable holes transporting material from the research and determine main parameters of these SC.

1.4. Statements to defend.

- In phenothiazine based hydrazones changing methyl- groups into phenyl- groups have no influence on holes drift mobility and ionization potential, but additional aromatic group in carbazole-based hydrazones increases holes drift mobility and ionization potential.
- Based on XTOF, ionization potential, photoluminescence measurements and characterization of experimental Solar cells, carbazole diamine V997 may be used as hole-transporting material in SC instead of Spiro-OMeTAD
- Internal quantum efficiency in experimental Solar cells containing investigated dyes depends on light quanta energy and reaches maximum at a point, which is $0.3\,\mathrm{eV}$ further from absorption edge.

1.5. Authors submissions

All investigated hole-transporting materials and dyes were synthesized at Kaunas University of Technology at Organic chemistry department. Dye-sensitized Solar cells were

made at *trinamiX*, IPCE and absorption measurements were undertaken at *trinamiX* as well.

Author of this dissertation has prepared PSCs containing experimental hole-transporting material, undertaken ionization potential measurements, hole drift mobility measurements using XTOF technique, as well an absorption of dyes on different substrates measurements.s

1.6. Novelty

Dye-sensitized solar cells (DSSCs) have attracted significant attention as an appealing alternative to conventional semiconductor photovoltaic devices, [1, 2] promising to offer a solution to low-cost large-area photovoltaic applications. DSSCs are fabricated from cheap, easily processable materials, deriving their competitive performance from judicious molecular design and control of nanoarchitecture.

Ruthenium complexes as molecular sensitizers have shown impressive solar-to-electric power conversion efficiencies (PCE) in liquid electrolyte based devices, with the PCE reaching over 11% under standard AM1.5G full sunlight. [3–7] Another type of sensitizers that demonstrated impressive performance in liquid electrolyte based devices are dyes based on porphyrin zinc complex. Porphyrin-sensitized DSSC with cobalt (II/III)–based redox electrolyte have achieved nearly 13% efficiency. [8]

In recent years, metal-free organic dyes have attracted increasing attention as they do not contain any toxic or costly metal and their properties are easily tuned by facile structural modification. To date the most efficient metal-free organic dyes for DSSCs were based upon the D–A architecture. With this construction it is easy to design new dye structures, extend the absorption spectra, adjust the energy levels and complete the intramolecular charge separation. DSSCs employing organic dyes featuring an electron donor and acceptor moiety connected by a π-conjugation bridge have reached 10% efficiency with liquid electrolytes [9–11] and up to 7% with solid HTM. [12–14] Recently it was demonstrated that large PCE increase, up to 12.75%, is achieved using sensitizers of the D-A-π-A design and careful structure optimization. [15]

In order to make the right choice of the materials for DSSC development, knowledge of the energy levels of the molecules is necessary. While the HOMO level could be determined directly by the measurement of the ionization potential (Ip) or from cyclic voltammetry data, the UV absorption spectra are needed to find the LUMO level. Energy levels are dependent on the aggregate state and environment of the dye molecules. In a solution, the dye molecules are surrounded by the solvent and in the layers they are contacting with

the molecules of the same material. Adsorbed on TiO_2 they interact with the TiO_2 surface to which they are chemically bound. The dye molecules can form aggregates and this process may also influence their energetic levels. So far, the ionization potential, using the photoemission in air method, was determined only in the layers of pure dyes, I_p values of the dyes adsorbed on TiO_2 are not known.

In this work energy levels of a number of hydrazone dyes are determined using photoemission in air, calculation from UV-Vis absorption spectrum edge and cyclic voltammetry techniques. The measurements are done in different environments (solution, thin solid film, dye adsorbed on nanoporous TiO_2) and the obtained results are evaluated and compared. The absorbed photon conversion to current efficiency (APCE) of the solar cells was also evaluated and compared with the incident photon quantum efficiency (IPCE) results.

1.7. List of articles and conferences

1.7.1. Articles related to this work

- A. Bieliauskas, V. Martynaitis, V. Getautis, T. Malinauskas, V. Jankauskas, E. Kamarauskas, W. Holzer, A. Šačkus, Synthesis of electroactive hydrazones derived from 3-(10-alkyl-10H-phenothiazin-3-yl)-2-propenals and their corresponding 3,3′-bispropenals, Tetrahedron **68**(18), 3552–3559 (2012).

- V. Gaidelis, E. Kamarauskas, T. Malinauskas, V. Getautis, R. Send, H. Wonneberger, I. Bruder, Relationship between measurement conditions and energy levels in the organic dyes used in dye-sensitized solar cells, RSC Adv. **5**(101), 82859–82864 (2015)

- A. Bieliauskas, V. Getautis, V. Martynaitis, V. Jankauskas, E. Kamarauskas, S. Krikštolaitytė, A. Šačkus, Synthesis of electroactive hydrazones derived from carbazolyl-based 2-propenals for optoelectronics, Synthetic Metals **179**, 27–33 (2013)

- A. Magomedov, N. Sakai, E. Kamarauskas, M. Franckevičius, G. Jokubauskaitė, V. Jankauskas, H. J. Snaith, V. Getautis, Amorphous hole transporting material based on 2,2‘- bissubstituted 1,1‘-biphenyl scaffold for application in perovskite solar cells, Chemistry – An Asian Journal **n/a–n/a** (2017).

1.7.2. Other articles

- E. Zaleckas, R. Griniene, B. Stulpinaite, J. Grazulevicius, L. Liu, Z. Xie, E. Schab-Balcerzak, E. Kamarauskas, B. Zhang, S. Grigalevicius, Electroactive polymers con-

taining pendant harmane, phenoxazine or carbazole rings as host materials for OLEDs, Dyes and Pigments **108**, 121–125 (2014).

- K. Rakstys, A. Abate, M. I. Dar, P. Gao, V. Jankauskas, G. Jacopin, E. Kamarauskas, S. Kazim, S. Ahmad, M. Grätzel, M. K. Nazeeruddin, Triazatruxene-based hole transporting materials for highly efficient perovskite solar cells **137**(51), 16172–16178
- K. Rakstys, M. Saliba, P. Gao, P. Gratia, E. Kamarauskas, S. Paek, V. Jankauskas, M. K. Nazeeruddin, Highly efficient perovskite solar cells employing an easily attainable bifluorenylidene-based hole-transporting material **128**(26), 7590–7594
- T. Braukyla, N. Sakai, M. Daskeviciene, V. Jankauskas, E. Kamarauskas, T. Malinauskas, H. J. Snaith, V. Getautis, Synthesis and investigation of the v-shaped tröger′s base derivatives as hole-transporting materials **11**(14), 2049–2056.

1.7.3. Posters in conferences related to this work

- Egidijus Kamarauskas, Gabrielė Jokubauskaitė, Artiom Magomedov, Vytautas Getautis, Valentas Gaidelis, Vygintas Jankauskas, A new hole transporting material for perovskite based Solar cells, *EMRS2016 Spring Meeting* (2016).
- Egidijus Kamarauskas, Tadas Malinauskas , Vytautas Getautis, Valentas Gaidelis, Impact of Measurement Conditions to Energy Levels in the Organic Dyes Used in Dye-Sensitized Solar Cells, *HOPV16* (2016).

1.7.4. Other posters

- Valentas Gaidelis, Vygintas Jankauskas, Egidijus Kamarauskas, The method of investigation of the semiconductor layers, *LNFK 40*(2013)

2. Experimental details

2.1. Details of measurements and calculations

Absorption measurements. UV spectra of the dye solutions were recorded on a Perkin Elmer Lambda 35 spectrometer. A concentration of 10^{-4} M solution of investigated dye in $CHCl_3$ and a microcell with an internal width of 1 mm was used. For the investigation of the absorption spectra of the films, the dyes were dissolved in tetrahydrofuran at concentration of 0.5 mg/ml, coated on the Corning glass substrate and dried at 60° C temperature for 5 minutes under ambient conditions. The measurements were carried out with the Avantes AvaSpec ULS-2048 spectrophotometer.

Ionization potential measurements. The ionization potential (I_p) was measured by electron photoemission in air. Samples for the measurements were prepared by dissolving dyes in tetrahydrofuran at concentration 8 mg/ml. The solutions were coated on an aluminized polyester substrate with a sub-layer of methylmethacrylate and methacrylic acid. The role of the sublayer was to improve adhesion of the sample material, to retard crystallization and to eliminate the electron photoemission from the Al layer through possible sample layer defects. In addition, the adhesion sub-layer was conductive enough to avoid charge accumulation on it during measurement. The thickness of both the sub-layer and the sample layer was 0.4 μm. The ionization potential was measured by the electron photoemission in air method similar to that described in. [16] The samples were illuminated with monochromatic light from the quartz monochromator with a deuterium lamp source. The negative voltage of -300 V was supplied to the sample substrate. The counter-electrode with the 4.5x15 mm^2 slit for illumination was placed at 8 mm distance from the sample surface. The counter-electrode was connected to the input of the BK2-16 type electrometer, working in the charge accumulation mode. A 10^{-15} – 10^{-12} A photocurrent was flowing in the circuit under illumination. This photocurrent I is strongly dependent on the incident light photon energy hν. The dependence of the square root of photocurrent on incident light quanta $I^{0.5} = f(h\nu)$ energy is well described by a linear relationship near the threshold, the letter indicating the I_p value.

Calculation of the absorbed photon conversion-to-current efficiency (APCE). APCE was calculated using the IPCE (incident photon conversion-to-current efficiency) data determined earlier. [17–19] The quantity of light absorbed in the photoactive layers of the cell L_{abs} is needed to calculate the APCE. The incident light is partly reflected from the cell, partly absorbed in the FTO and TiO_2 layers. Before reaching the active layer the light undergoes interference caused by the light reflections from the TiO_2 layer surfaces. This causes the meandering of the absorption spectra, especially in the regions of weak absorption; it was smoothed by the Lorentz approximation of the Origin program. After reaching the Ag anode light is reflected back into the active layers of the cell, this increases the light absorption by the dye. These phenomena were taken into account while calculating the amount of the light absorbed in the photoactive layers L_{abs}, which is expressed by the formula:

$$L_{abs} = 10^{-D_r}(1 - 10^{-2(D-D_r)}) \tag{2.1}$$

Where D_r is the absorbance of the SC in the red region of the spectrum where there is no light absorption by the dye and D is the absorbance at a given wavelength. The values of APCE were found dividing the values of IPCE by L_{abs}.

The main source of the APCE evaluation error is caused by the meandering of the absorbance, which leads to the inaccuracy of the D_r of ± 0.01. In Figure 3 the APCE values are calculated using D_r equal to the Lorentz approximation at 750 nm. The ends of the error bars correspond to the APCE values calculated using the D_r values by 0.01 larger or smaller. The APCE evaluation error increases with decreasing cell absorbance making evaluation practically impossible at wave lengths more than 700 nm.

Cyclic voltammetry (CV) measurements. The electrochemical studies were carried out by a three-electrode assembly cell from Bio-Logic SAS and a micro-AUTOLAB Type III potentiostat-galvanostat. The measurements were carried out with a glassy carbon electrode in dichloromethane solutions containing 0.1 M tetrabutylammonium hexafluorophosphate as electrolyte, $Ag/AgNO_3$ as the reference electrode and a Pt wire counter electrode.

Potentials measured vs. Fc^+/Fc were converted to NHE by addition of +0.69 V [20] and the NHE vs. the vacuum level to 4.5 V. [21] The ionization potential (I_p^{CV}) and electron affinity (E_A^{CV}) levels were calculated according to the formula $I_p^{CV} = -(E_{ox} + 5.19)$ eV and $E_A^{CV} = -(E_{red} + 5.19)$ eV, where E_{ox} and E_{red} are oxidation and reduction potentials respectively.

2.2. Preparation of samples

Fabrication of samples fro ionization measurements For the I_p investigation of the dyes on TiO_2, the FTO glasses were cleaned and coated with the Ti Nanoxide T/SC titania paste from Solaronix using spin coating technique. The titania paste was coated at 1000 rpm for 30 sec and sintered at 460° C temperature for 30 minutes. A thickness of TiO_2 layer was approximately 100 nm. The dyes were dissolved in tetrahydrofuran at concentration 0.5 mg/ml. The FTO glasses with TiO_2 layer were dipped in dye solutions for 12 hours and dried at 60°C temperature for 5 minutes.

Fabrication and Characterization of the Solid-State Dye-Sensitized Solar-Cells. A TiO_2 blocking layer was prepared on a fluorine-doped tin oxide (FTO)-covered glass substrate using spray pyrolysis. [22] Next, a TiO_2 paste (Dyesol), diluted with terpineol, was applied by screen printing, resulting in a film thickness of 1.7 μm. All films were then sintered for 45 min at 450 °C, followed by treatment in a 40 mM aqueous solution of $TiCl_4$ at 60 °C for 30 min, followed by another sintering step. The prepared samples with TiO_2 layers were pretreated with 5 mM solutions of 2-(p-butoxyphenyl)acetohydroxamic acid sodium salt or 2-(p-butoxyphenyl)acetohydroxamic acid tetrabutylammonium salt in ethanol. The electrodes were then dyed in 0.5 mM dye solution in CH_2Cl_2. Spiro-MeOTAD was applied by spin-coating from a solution in DCM (200 mg/ml) also containing 20 mM $Li(CF_3SO_2)_2N$. Fabrication of the device was completed by evaporation of 200 nm of silver as the counter electrode. The active area of the ssDSSC was defined by the size of these contacts (0.13 cm^2), and the cells were masked by an aperture of the same area for measurements. The Current–voltage characteristics for all cells were measured with a Keithley 2400 under 1000 W/m^2, AM 1.5G conditions (LOT ORIEL 450 W). The incident photon to current conversion efficiencies (IPCE) were obtained with an Acton Research Monochromator using additional white background light illumination.

Fabrication of the perovskite Solar cells using FTO/c-TiO_2/m-TiO_2/$MAPbI_3$/HTM/Au architecture . Fluorine-doped tin oxide (FTO) glasses (Solaronix©) were patterned by etching with Zn powder and HCl diluted in distilled water. The etched substrates were then cleaned with distiled water ,acetone, isopropanol and then dried in air. Compact TiO_2 hole-blocking layer was deposited by spray-pyrolysis onto glasses on hotplate at 450°C using titanium(IV) propoxide diluted in acetylacetone and isopropanol. Mesoporous TiO_2 layer was spin-coated from titanium pasta (Dyesol©) dissolved in isopropanol in 2:7 mass ratio. Layer was then sintered in the air at 550°C for 1 hour. A PbI_2 layer was then deposited by spin-coating from 1.1M solution in dimethylformamide with a spin-coating speed of 5000

rpm and immersed into 0.06M methylammonium solution in isopropanol for 10 seconds. Obtained perovskite layer was then annealed at 100°C for 30 minutes in inert atmosphere. Hole-transporting layer was deposited by spin-coating using a solution containing 0.06 mol hole -transporting material solution in chlorobenzene, 330 mol% of 4-tertbutylpyridine and 50 mol% of LiTFSI as additives. This layer was spin-coated with a spin-coating speed of 2000 rpm. Au contacts were evaporated onto hole-transporting layer and the complete device was encapsulated in inert atmosphere.

3. Results and discussion

3.1. Investigated hole-transporting materials

All investigated hole-transporting materials were synthesized at Kaunas University of Technology, by professors A. Šackus and V. Getautis and their groups.

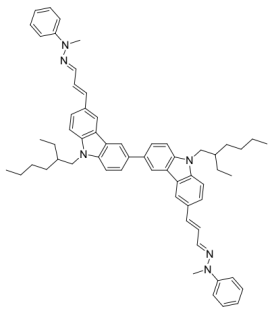

(a) **8a**

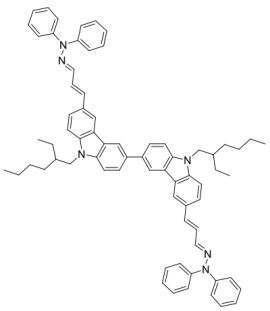

(b) **8b**

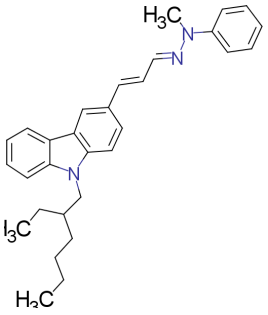

(c) **4a**

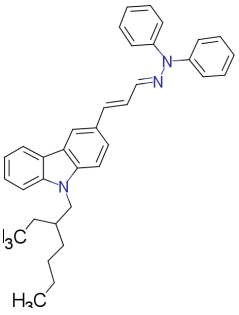

(d) **4b**

Figure 3.1.: Electro-active carbazole-based hydrazones

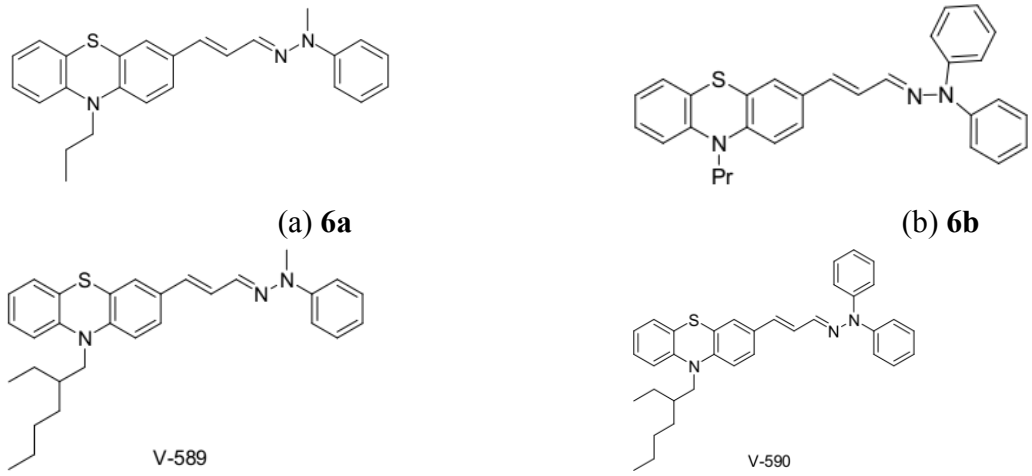

(a) **6a** (b) **6b**

(c) **6c** (d) **6d**

Figure 3.2.: Electro-active phenothiazine-based hydrazones

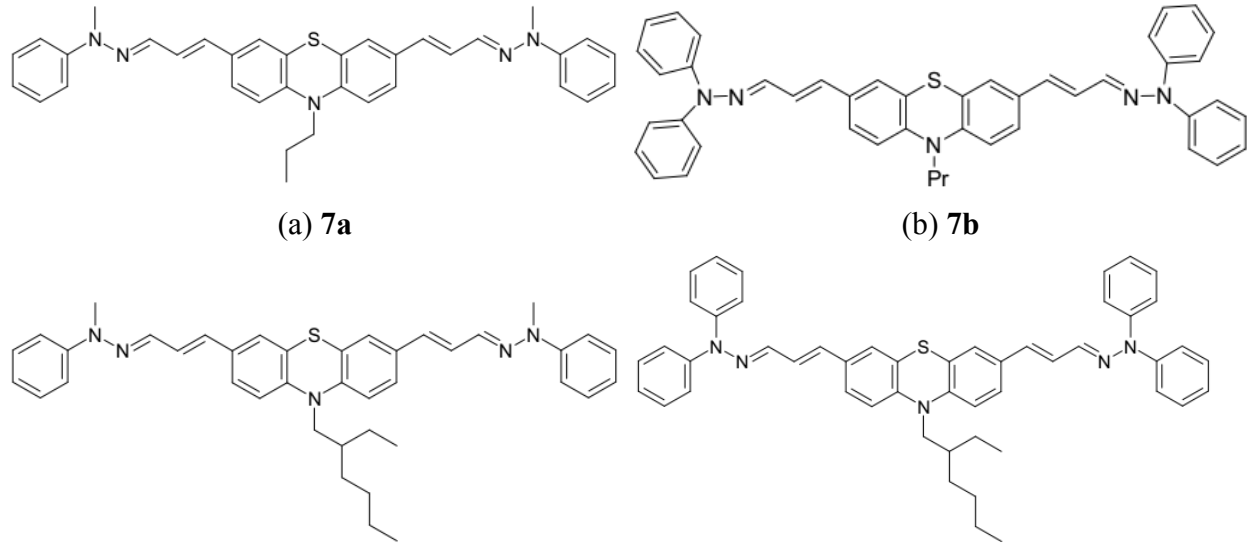

(a) **7a** (b) **7b**

(c) **7c** (d) **7d**

Figure 3.3.: Electro-active phenothiazine-based hydrazones

3.1.1. Hole drift mobility measurements by XTOF

All these materials were investigated using XTOF method in order to determine their main charge carriers and mobilities of these carriers. We found that main charge carrier in all these materials is holes (see fig. S1, S2). We found also that all mobilities fall into

same case and can be described by Pool-Frenkel equation:

$$\mu = \mu_0 \mathrm{e}^{\alpha\sqrt{E}} \tag{3.1}$$

It means that such dependence on electrical field can be explained by Bässler formalism: [23]

$$\mu(E,T) = \mu_0^{'} \exp\left[-\left(\frac{2\sigma}{3kT}\right)^2\right] \exp\left\{C\left[\left(\frac{2\sigma}{3kT}\right)^2 - \Sigma^2\right] E^{\frac{1}{2}}\right\} \tag{3.2}$$

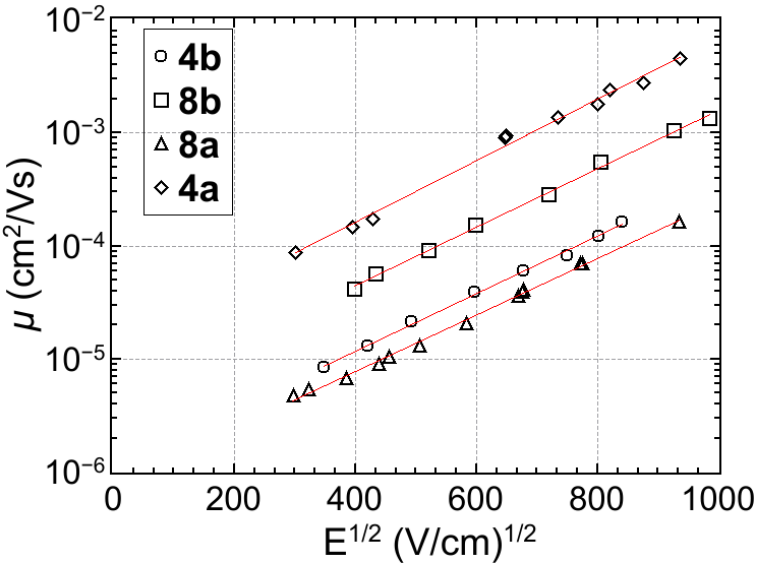

Figure 3.4.: The dependency of hole drift mobility on squared E

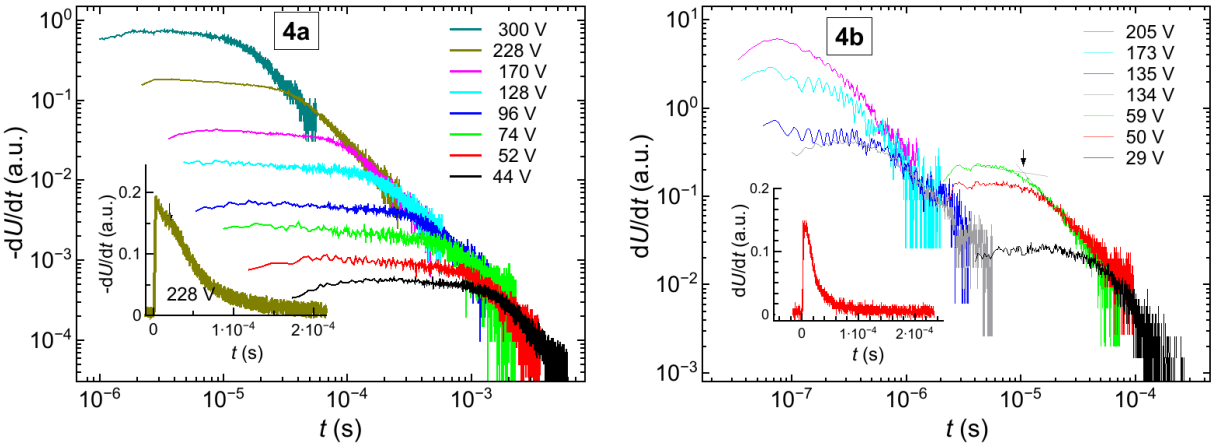

(a) (b)

Figure 3.5.: a) **4a** kinetics of hole drift mobility b) **4b** kinetics of hole drift mobility

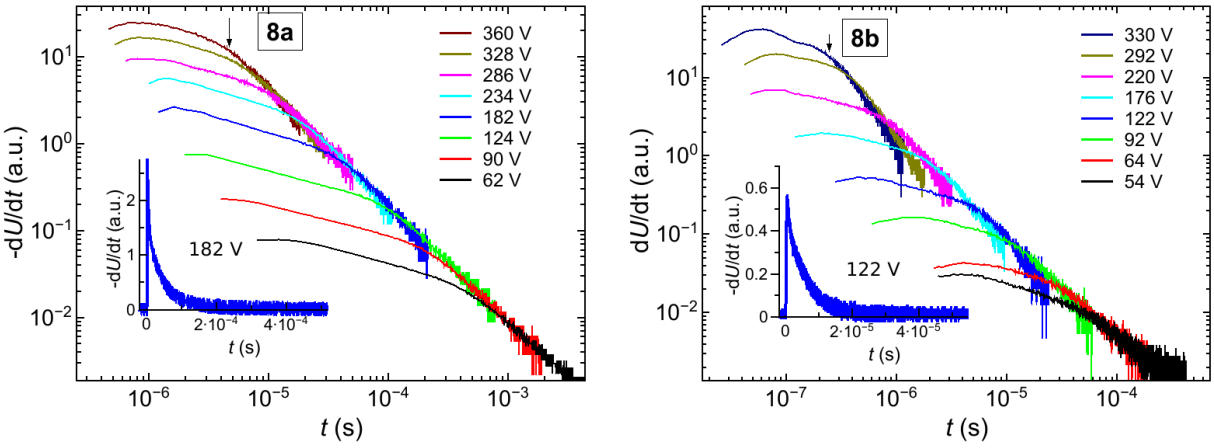

(a) (b)

Figure 3.6.: a) **8a** kinetics of hole drift mobility b) **8b** kinetics of hole drift mobility

It can be seen from XTOF measurements, that an additional aromatic group in **4a**, **4b**, **8a** and **8b** moieties increased drift mobility and ionization potential. Full summary of measurements results can be found in table 3.1. The best result and biggest impact of additional aromatic group is seen in **4b** moiety and it can be explained, that this moiety has a more compact structure than others, thus distance between molecules in layers ot that moiety is much more smaller in comparison to others.

Ionization potential increased also, by adding additional aromatic group (See fig. 3.8 or a table 3.1)

Table 3.1.: Hole drift mobilities and ionization potentials I_p in pure **4a**, **4b**, **8a**, **8b** materials

HTM	d, μm	μ_0, $cm^2/(Vs)$	μ, $cm^2/(Vs)$	I_p,eV	α, $(cm/V)^{0,5}$
4a	5	8×10^{-7}	2.4×10^{-4}	5.24	0.0058
4b	3.2	1.3×10^{-5}	7×10^{-3}	5.28	0.0063
8a	5.1	1.1×10^{-6}	4×10^{-4}	5.15	0.0059
8b	3.4	4.2×10^{-6}	1.6×10^{-3}	5.22	0.0060

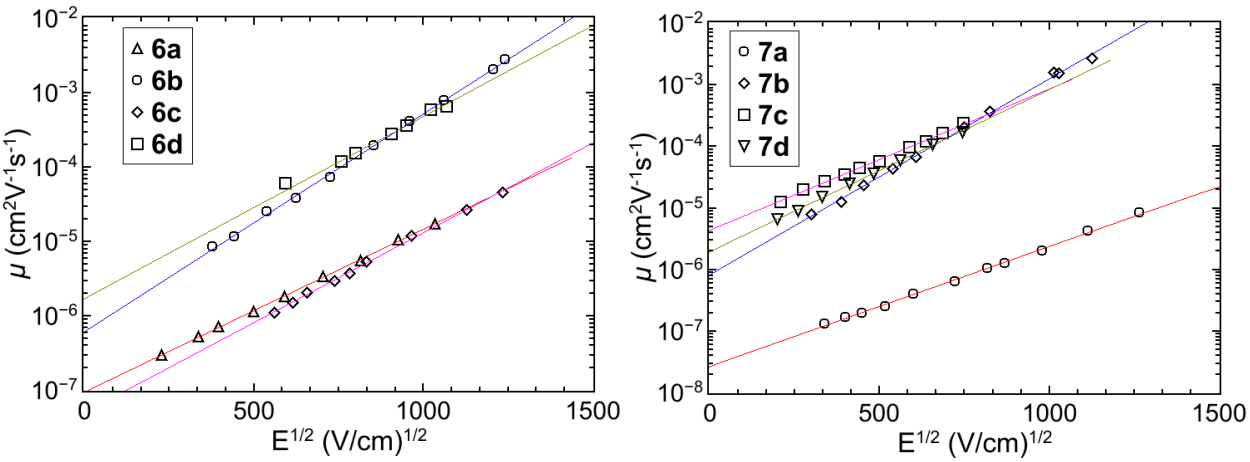

(a) (b)

Figure 3.7.: a) The dependence of hole drift mobility μ on electrical field E in materials **6a**, **6b**, **6c**, **6d**, b) The dependence of hole drift mobility μ on electrical field E in materials **7a**, **7b**, **7c**, **7d**

There was not a big difference in hole drift mobilities in next all eight materials (**6a**, **6b**, **6c** and **6d**, as well in **7a**, **7b**, **7c** and **7d**) , thus we can make a statement, that in those phenothiazine-based hydrazones an additional aromatic group does not have impact on hole drift mobility values.

Table 3.2.: Values of hole drift mobility in materials **6a**, **6b**, **6c**, **6d**, **7a**, **7b**, **7c** ir **7d**

HTM	d, μm	μ_0, cm^2/Vs	μ, cm^2/Vs	α, $cm^{0,5}V^{0,5}$
6a	7	2.0×10^{-6}	5.5×10^{-4}	0.0056
6a+PC-Z, 1:1	10	9.5×10^{-8}	1.6×10^{-5}	0.0051
6b	3.6	0.6×10^{-6}	5.4×10^{-4}	0.0068
6c+PC-Z, 1:1	5.5	5.0×10^{-8}	1.3×10^{-5}	0.0056
6d	3.2	1.7×10^{-6}	4.6×10^{-4}	0.0056
6d+PC-Z, 1:1	5.2	2.7×10^{-7}	1.76×10^{-5}	0.0044
7a+PC-Z, 1:3	6.0	2.7×10^{-8}	2.4×10^{-6}	0.0045
7b	3.8	0.8×10^{-6}	1.3×10^{-3}	0.0073
7b+PC-Z, 1:1	5.0	9.8×10^{-8}	9.2×10^{-5}	0.0069
7c	3.7	4.4×10^{-6}	9×10^{-4}	0.0053
7d	5.1	1.9×10^{-6}	8×10^{-4}	0.0061

3.1.2. Measurements of ionization potentials

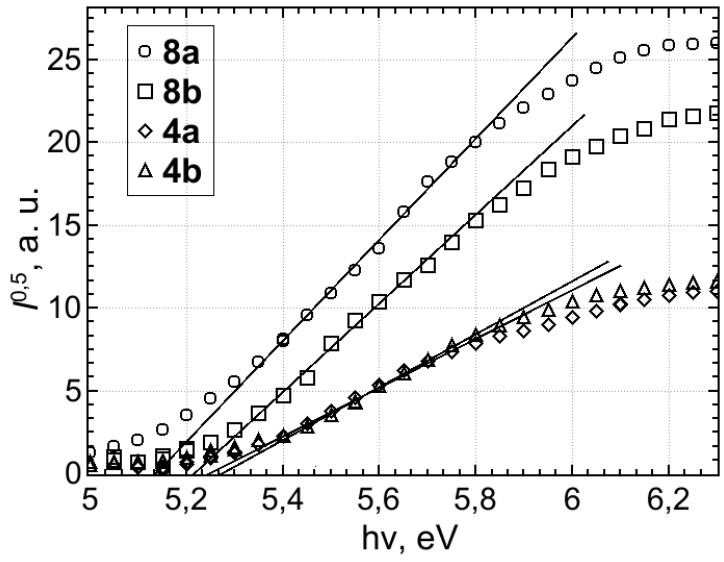

Figure 3.8.: Photoelectrons emission spectra in **4a**, **4b**, **8a** and **8b**

We can see from above picture (fig. 3.8), that additional aromatic group increases ionization potential a little bit in series of 4th and 8th materials. It could be explained in this way, that additional π-conjugated system holds stronger electrons and thus we need more energy to extract them from molecules (to ionize those molecules).

Table 3.3.: Ionization potentials I_p in **6a**, **6b**, **6c**, **6d** and **7a**, **7b**, **7c**, **7d** materials.

HTM	I_p, eV	HTM	I_p, eV	HTM	I_p, eV	HTM	I_p, eV
6a	5.25	**6b**	5.28	**6c**	5.30	**6d**	5.35
7a	5.12	**7b**	5.15	**7c**	5.18	**7d**	5.22

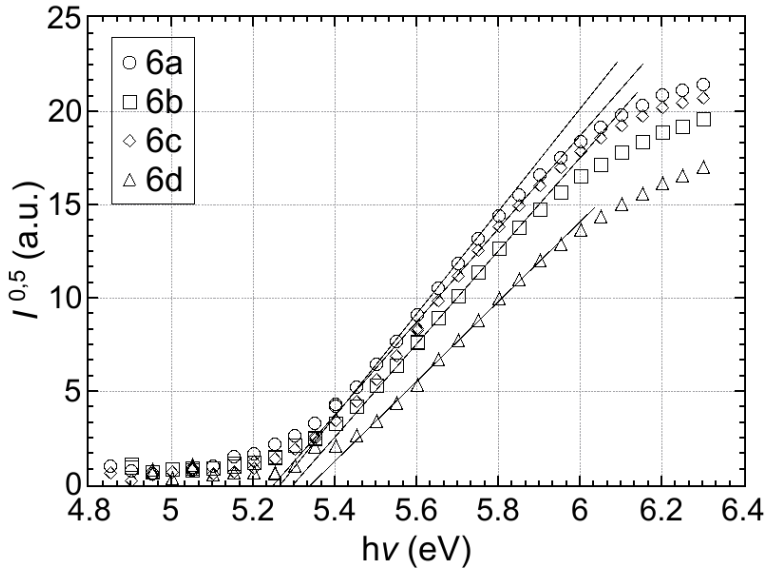

Figure 3.9.: Photoelectrons emission spectra in **6a**, **6b**, **6c**, **6d**

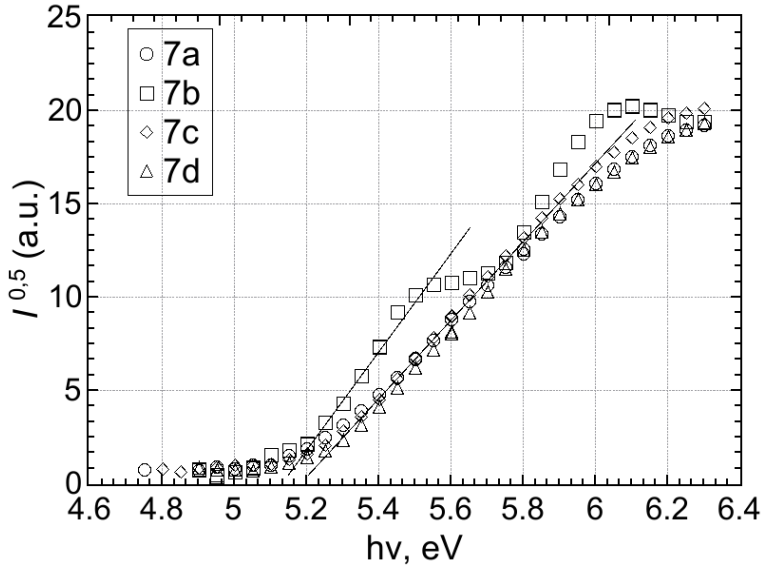

Figure 3.10.: Photoelectrons emission spectra in **7a**, **7b**, **7c**, **7d**

It can be seen from photoelectrons emission spectra, that additional aromatic groups in series of 6th and 7th materials do not have impact on ionization potential also.

3.2. PSC containing V997 as hole transporting material

The carbazole-based hole-transporting material V997 was synthesized as a replacement for commercial but very expensive hole-transporting material, so called Spiro-OMeTAD. In this work we tried to determine its properties and its ability to work in Solar cells as well.

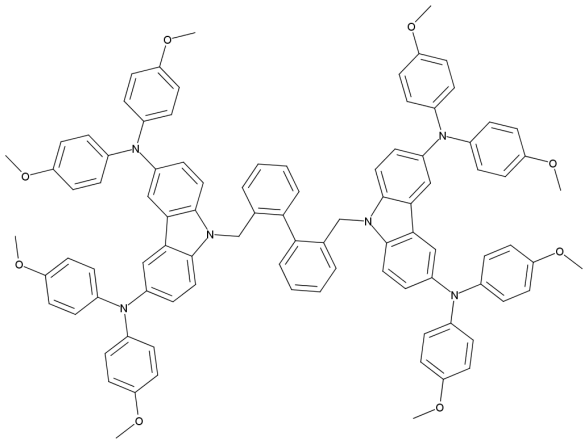

Figure 3.11.: Structure of carbazole-based hole-transporting material V997

3.2.1. Hole drift mobility measurements using XTOF technique

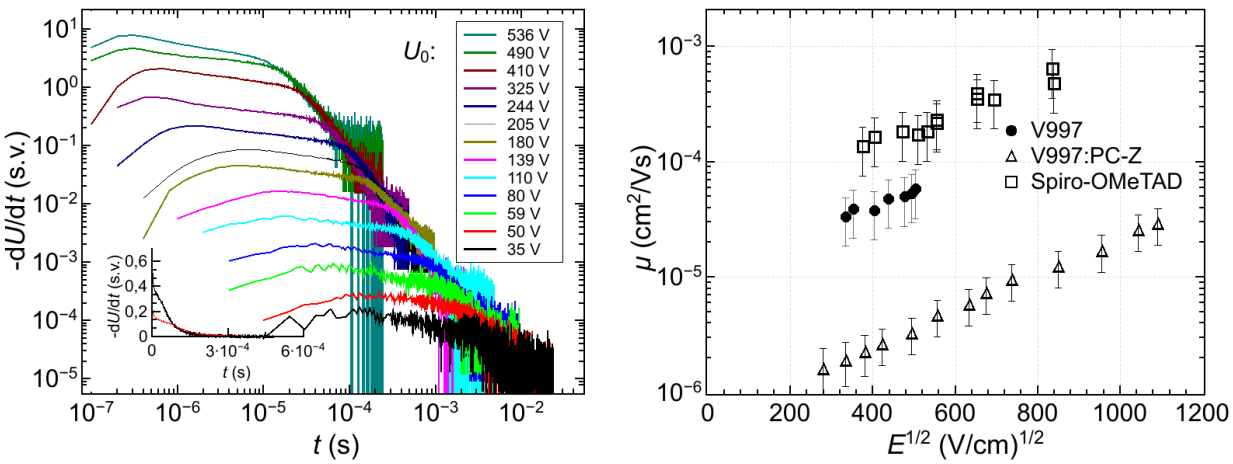

(a) (b)

Figure 3.12.: a) - XTOF drift currents in V997 with PC-Z as a binder, λ=337 nm, t=1 ns, b) - Dependency of hole-drift mobility on electric field E in V997 and Spiro-OMeTAD materials.

As it can be seen from XTOF measurements, V997 material has a lit bit lower hole drift mobility in comparison with Spiro-OMeTAD, thus we can expect a little bit lower short-circuit current from cells containing V997 than from cells made with Spiro-OMeTAD. [24]

3.2.2. Absorbtion spactra measurements in V997

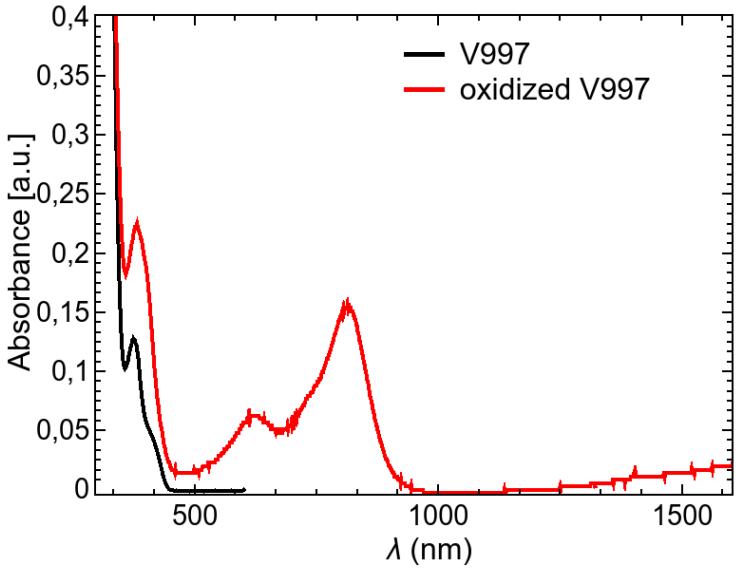

Figure 3.13.: Uv/Vis/Nir absorption spectra of V997 and chemically oxidized (with 1 eq. of AgTFSI) V997.

The UV-Vis absorption spectrum of pristine and oxidized form of V997 in THF solution is shown in Fig. 2a. In its pristine form V997 shows absorption band with the maximum at 300 nm, while no absorption is observed in the visible spectral range. This confirms that conjugation between two dimethoxydiphenylamine substituted carbazole fragments is absent. Although HTM in the perovskite solar cell is always used in the partly oxidized form [25] , thus the new HTM was chemically oxidized with silver bis(trifluoromethylsulphonyl)imide (AgTFSI). The absorption of oxidized V997 form ($V997^{2+}(TFSI^{-})_2$) results in two additional absorption bands with main peaks at 620 and 800 nm, and also broad band with the maximum over 1600 nm, whose presence is attributed to the formation of the mixed-valence species [26] and shows electron transfer processes in the molecule.

3.2.3. Ionization potential measurements

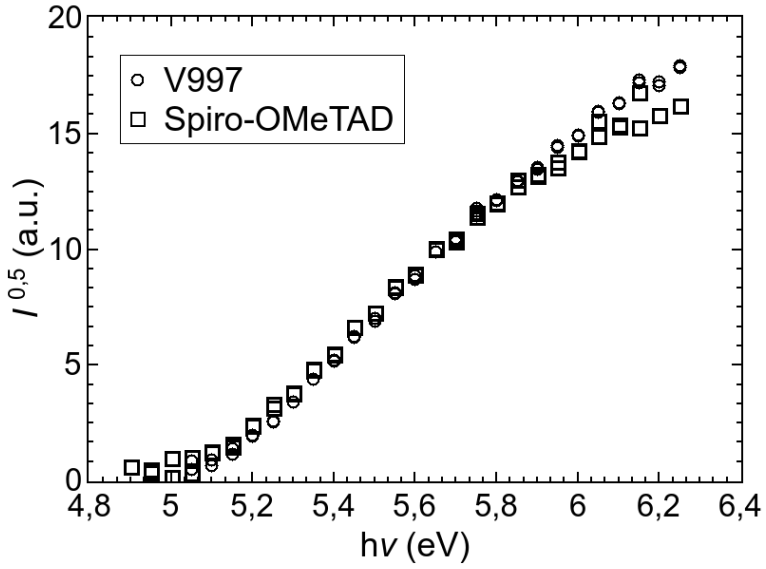

Figure 3.14.: Photoelectrons emission spectra in V997 and Spiro-OMeTAD materials

In order to determine HOMO (highest occupied molecular orbital) energy level of V997, solid state ionization potential (I_p) was measured by photoelectron spectroscopy in air (PESA) method. The HOMO energy level value of V997 was determined to be -5.1 eV (Figure 3.14). Compared with the energy level of $CH_3NH_3PbI_3$ perovskite and gold work function, the estimated $I_p$value for V997 is compatible for application in perovskite solar cell devices to ensure efficient hole transfer at the interface.

Table 3.4.: Comparison of hole drift mobilities and ionization materials in V997 and Spiro-OMeTAD

Material	μ_0, cm/Vs^2	μ, cm/Vs^2	I_p
V997	1.3×10^{-5}	1.3×10^{-4}	5.1
Spiro-OMeTAD	4×10^{-5}	5×10^{-4}	5.0

3.2.4. Time resolved photoluminescence measurements

Time resolved photoluminescence (PL) measurements were undertaken to study charge carrier dynamics in perovskite films employing hole transporting V997 and Spiro-OMeTAD

layers . The PL decay kinetics of neat perovskite film show single-exponential decay with a lifetime of several tens of nanoseconds. A slow PL decay component we attribute to the bimolecular nongeminate electron-hole recombination. As is expected, charge carrier recombination is dominating radiative channel in the neat perovskite films. Conversely, significant PL quenching is observed when perovskite is interfaced with Spiro-OMeTAD and V997 hole transporting materials (blue and red curves in 3.15b).

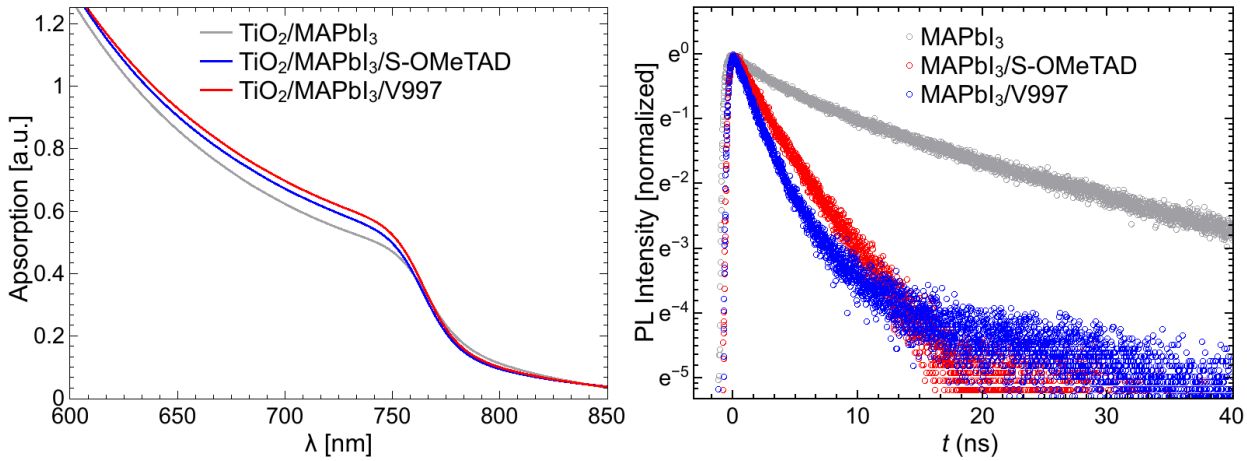

(a) (b)

Figure 3.15.: a) UV-vis absorption spectra of TiO_2/perovskite film (gray) and perovskite deposited with Spiro-OMeTAD (blue) and V997 (red) hole transporting materials b) Photoluminescence decay kinetics of lead halide perovskite films deposited on glass substrates comprising Spiro-OMeTAD (blue) and V997 (red) hole transporting and insulating PMMA layers (gray). Photoluminescence lifetimes were monitored at the emission maximum at 770 nm upon excitation at 470 nm

3.2.5. Main parameters of perovskite Solar cells containing V997 as hole transporting material

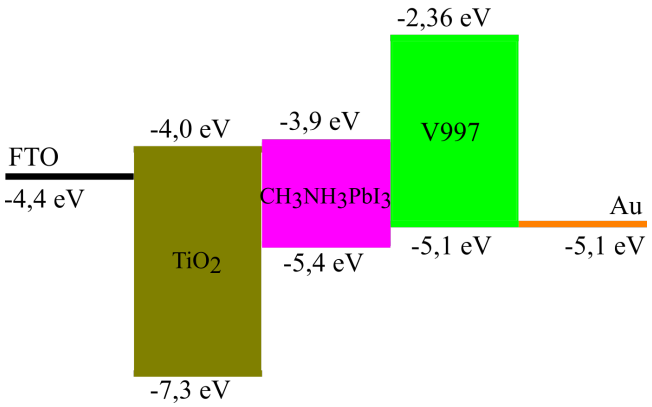

Figure 3.16.: Diagram of energy levels of PSC containing V997 as hole transporting material

As shown in picture 3.16, all energetic levels are compatible to each other.

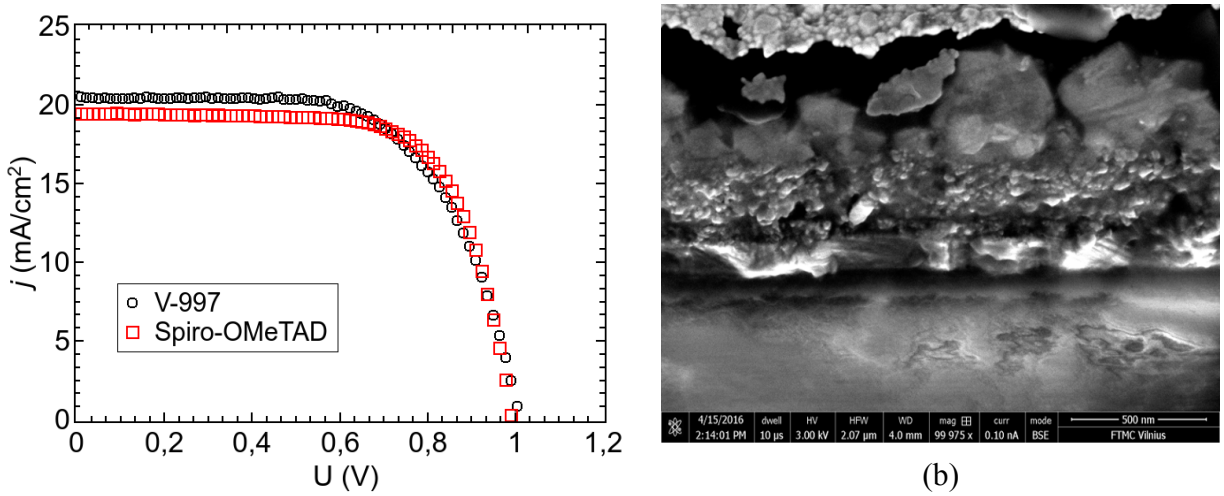

Figure 3.17.: a) - J-V curves of the best performing SC, b) - SEM image of PSC containing V997.

As shown in 3.17a fig., V997 performed as well as Spiro-OMeTAD. Main parameters

are listed in table 3.5. We can see, that all parameters are comparable to each other, and efficiency (PCE) is almost equal.

Table 3.5.: Main parameters of best PSC

HTM	j_{sc}, mA/cm^2	U_{oc},V	FF	PCE,%
Spiro-OMeTAD	19.5	0.99	0.69	13.46
V997	20.5	1.004	0.63	13.00

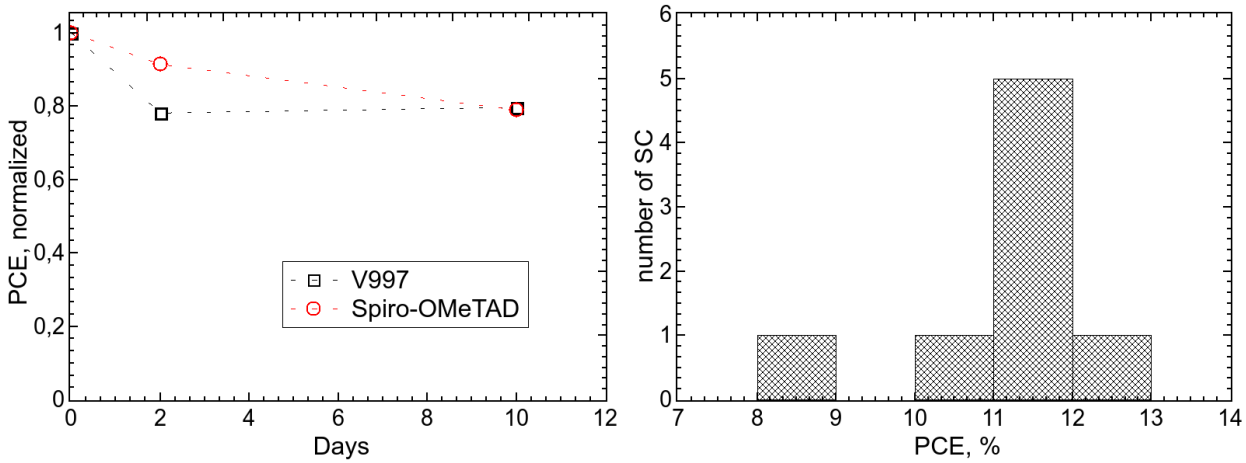

(a) (b)

Figure 3.18.: a) Decay curves of PSC containing V997 or Spiro-OMeTAD as hole transporting material, b) Distribution of PCE.

We have tested stability of perovskite-based Solar cells containing V997 or Spiro-OMeTAD and we have found that both was quite stable (fig. 3.18a), and stability for a few days was almost equal for both cells.

Table 3.6.: Comparison of synthesis cost

HTM	Cost of synthesis, €·g^{-1}	Commercial price, €·g^{-1}
Spiro-OMeTAD	82.64 [27]	200 – 300
V997	13.87	n/a

3.3. The dyes investigated

The investigated hydrazone dyes **D1**–**D9** (Figure 3.19) have been synthesized by the procedures reported earlier. [17–19]

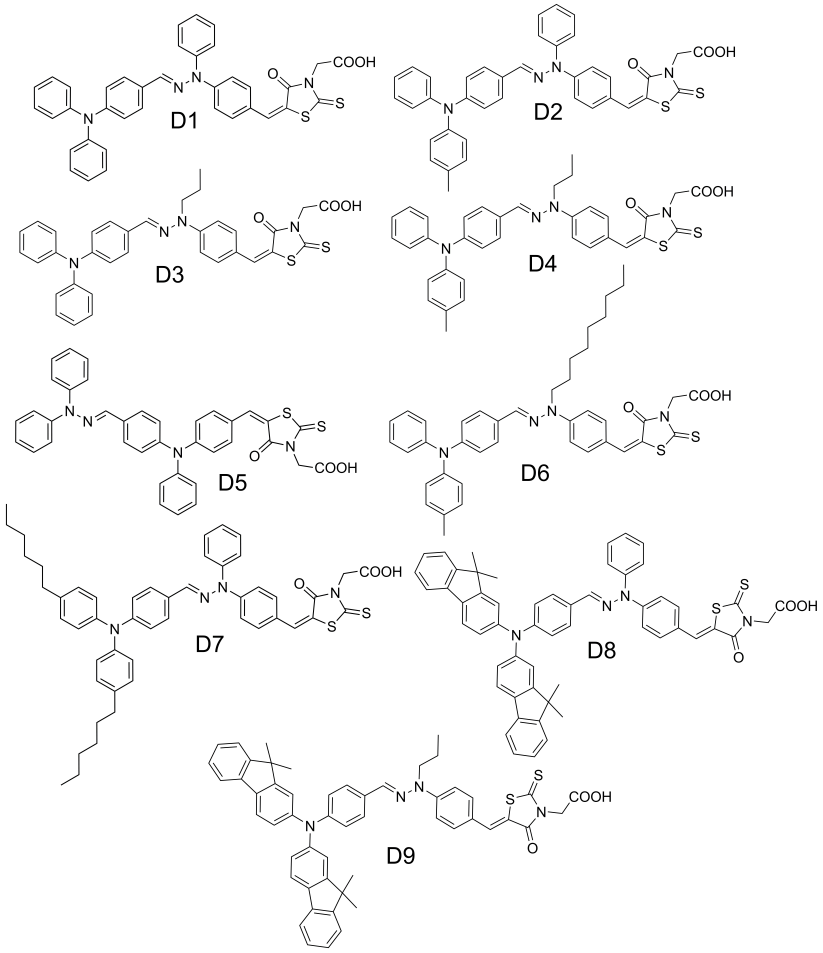

Figure 3.19.: Structures of the investigated hydrazone dyes **D1**–**D9**.

3.3.1. Energy levels of the investigated dyes

The ionization potentials of the hydrazone dyes **D1**–**D9** have been measured using cyclic voltammetry and photoemission in air techniques, while the electron affinity was measured by cyclic voltammetry and determined from the band edges of the absorption spectra.

The absorption spectra of the dyes were investigated in solution, in a thin layer of dye on glass and in solar cells before the deposition of the Ag electrode. The results of the investigations for the dye **D7** are presented in Figure 3.20, spectra of the remaining materials could be found in the supplementary information. To better reveal the dependencies at the long wave end of the spectrum, the square root of the normalized absorbance or molar

extinction coefficient ϵ, in case of the dye solution, are plotted. For comparison the values of the square root of incident photon to current conversion efficiencies (IPCE), determined in constructed solid-state dye-sensitized solar cells (ssDSSC), are also presented. The long wave dependencies, as seen in Figure 3.20, can be approximated by two linear regions.

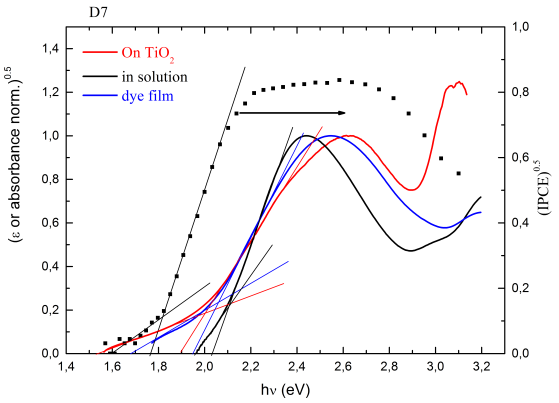

Figure 3.20.: The normalized adsorption spectra of **D7** in solution, film of the pure dye and adsorbed on TiO_2 in SC. The IPCE spectrum of the constructed SC is given for comparison.

The intersection of the straight lines with the abscise gives two long wave end values of the spectra, which are given in Table 1. In the case of the dye **D7** in solution, the intersection point gives the spectrum edge values 2.03 and 1.95 eV. The larger value may be ascribed to the stronger absorption band caused by the main mass of the dye molecules while the lower value is due to absorption by a few aggregated molecules. In case of the dye film or solar cell (SC) sample, these aggregation bands in the long wave region are stronger and the differences between the two intersections are larger. The increase of shoulder size in the long wave region of the absorption spectrum may be caused by the interactions between the dye molecules and the aggregate formation, which are weak in the solution, but much stronger in the film and between dye molecules adsorbed on TiO_2. In the case of some dyes, for example **D5** (Figure S9), shoulder in the long wave absorption region of the films could be very strong and the corresponding spectrum edges reach to about 1 eV. This may be caused not only by aggregation, but also by the presence of a crystalline phase in the films. The E_g measurement results, calculated from the edges of the absorption spectra (Table 1), show that dyes in the solution demonstrate the largest E_g values, exceeding those determined from the spectra of the films or dyes adsorbed on TiO_2. However, these are smaller than the ones found in the CV experiments, indicating that the aggregation is largest in the films, lower in the adsorbed on TiO_2 state and lowest in the solution.

Table 3.7.: E_g results from the CV measurements, long wave edges of the spectra of the dye solutions, films of pure dyes on glass substrates and in SC, the edges of IPCE spectra from the solar cell devices, as well as ssDSSC conversion efficiency under standard AM 1.5G illumination

Dye	CV, eV	Solution, eV	Film, eV	Cell, eV	IPCE, eV	η, %
D1	2.16	2.06	2.03 , 1.2	1.87 , 1,78	1.81 , 1.7	3.8
D2	2.09	2.01 , 1.9	1.88 , 1.7	1.89 , 1.65	1.77 , 1.7	3.7
D3	2.15	2.01 , 1.5	1.89 , 1.1	1.90 , 1.6	1.77 ,1.6	3.4
D4	2.12	2.02 , 1.8	1.85 , 1.65	1.89 , 1.6	1.73 , 1.6	3.2
D5	2.15	2.07 , 1.8	1.7 , 1.0	1.98 , 1.6	1.97 , 1.85	3.0
D6	2.10	2.03 , 1.75	1.83 , 1.0	1.92 , 1.6	1.81 , 1.7	3.9
D7	2.13	2.03 , 1.95	1.95 , 1.7	1.90 , 1.6	1.76 , 1.6	4.5
D8	2.09	2.01 , 1.95	1,89 , 1.2	1.93 , 1.6	1.84 , 1.6	3.8
D9	2.05	2.02 , 1.75	1.85 , 1.0	1.88 , 1.75	1.88 , 1.76	3.8

Looking at the energy levels determined using CV and photoemission in air techniques (Table 2), it is evident that absolute values differ quite noticeably, CV results are about 0.2–0.3 eV higher. The differences arise from different measurement conditions, CV is done in solution, while photoemission is measured in the solid film. Dependence between energy level and structure is more pronounced in the case of measurements done in the solution. Due to significant dilution dye molecules have a reduced tendency to form aggregates in the solution which could influence the position of the energy levels, additionally, the way molecules pack in the film is also a significant factor.

Table 3.8.: Ionization potential and electron affinity values of the investigated dyes

Dye	I_p^{CV}, eV	I_p of dye films, eV	I_p on TiO_2, eV	EA^{CV}, eV	EA of dye films, eV	EA on TiO_2, eV
D1	5.55	5.22	5.29	3.39	3.2 , 4.0	3.4 , 3.5
D2	5.47	5.04	5.09	3.38	3.2 , 3.3	3.2 , 3.4
D3	5.47	5.26	5.13	3.32	3.4 , 4.2	3.2 , 3.5
D4	5.44	5.13	5.06	3.32	3.3 , 3.5	3.2 , 3.5
D5	5.52	5.36	5.26	3.37	3.7 , 4.4	3.3 , 3.7
D6	5.46	5.31	5.17	3.36	3.5 , 4.3	3.25 , 3.6
D7	5.44	5.22	5.18	3.31	3.3 , 3.5	3.3 , 3.6
D8	5.47	5.17	5.17	3.38	3.3 , 4.0	3.2 , 3.6
D9	5.41	5.17	5.08	3.36	3.3 , 4.2	3.2 , 3.33

CV measurements reveal that substitution of aromatic moieties with aliphatic ones in

the hydrazone fragment reduces both I_p and electron affinity (EA), while modifications at the triphenylamine donor site affect only the I_p values. It has to be noted that the length of the aliphatic chains has a negligible effect on the energy levels of the dyes in the solution. In the solid state however, the molecules are much more prone to form aggregates and the structure/energy level relationship becomes a lot less predictable. Energy levels of the dye molecules adsorbed on the TiO_2 follow yet another pattern. Due to the different arrangement and intermolecular interactions of the molecules adsorbed on TiO_2, the I_p increases, compared to the one measured in the film, in the dyes **D1**, **D2**, **D9** containing a diphenylhydrazone moiety and decreases if the phenyl ring is substituted by the aliphatic fragment (**D3**, **D4**, **D6**, **D7**). Curiously, if longer aliphatic chains are used, the difference between I_p measured in film and on TiO_2 becomes smaller (**D7**) or non-existent (**D8**), indicating that longer aliphatic chains retard aggregate formation in the film.

Overall, this investigation shows that the degree of aggregation of the dyes in the films, in solutions and adsorbed on TiO_2 is different, so it may be incorrect to use the ionization potential results measured in the dye films for evaluation of the energy levels in the SC. It may also be incorrect to use the absorption spectrum edges measured for the dye films or solutions to evaluate the electron affinity EA level of the dyes in the solar cells. The better way to do this is to measure both ionization potential and absorption spectra for the dyes adsorbed on TiO_2, as it was done in this investigation.

3.3.2. IPCE and APCE

The efficiency of the investigated cells is 3 to 4.5 %, which is considerably less than achieved in the SC with liquid electrolytes. While a number of factors are important, one of the causes limiting efficiency may be improper tuning of the energy levels inside the cell. In order to better understand the causes limiting the conversion efficiency we investigated the spectrums of the absorbed photon conversion to current efficiency (APCE), or the quantum efficiency of the conversion process.

The long wave end of the IPCE spectrum coincides with the edge of the absorption spectrum of the cell, but differs from the edges in the solution. The edge of the IPCE spectrum of the investigated dyes usually is at lower quanta energy than the absorption edge in solution, indicating that the charge carrier generation in some cases takes place not only by the light absorption by single molecules of the dyes, but also by their aggregates. In some cases, as for the dyes **D2**, **D4**, **D7** (Figure 2, S4, S7) there is only a small difference between the edges of the absorption spectra in the film and IPCE, but in a number of other cases, as **D5**, **D3** (Figure S5, S11), the difference is significant. These observations show that not all the aggregation forms are present between the molecules adsorbed on TiO_2 or

take part in the charge carrier photogeneration process.

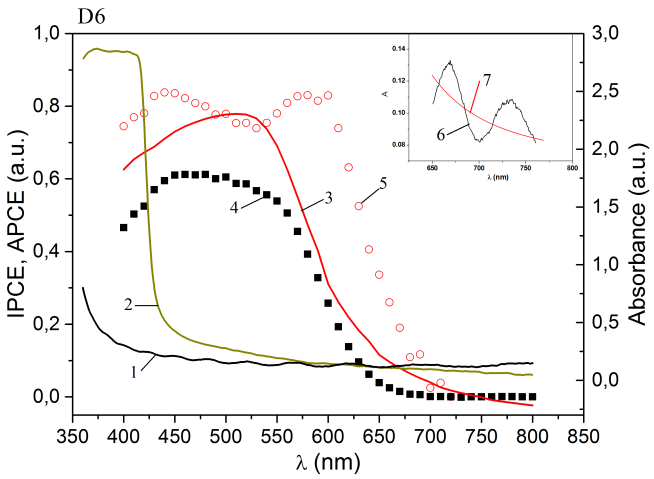

Figure 3.21.: The spectra of the SC with the dye **D6**. 1 -absorbance of the glass substrate with TiO_2 nanoporous layer, 2 - absorbance of the 2 μm thick spiro-MeOTAD with LiTFSI additive , 3 - quantity of the absorbed light by the active layers of the cell , 4 - IPCE, 5 - APCE.

From the data provided in Figure 3.21 it is evident that a significant light absorption by nanoporous TiO_2 takes place at the light wavelengths below 400 nm. Hole transporting material spiro-MeOTAD, doped with the LiTFSI, also contributes to overall absorption especially at wavelengths below 600 nm. The curve 3 shows the amount of the light absorbed in the active layers of the cell by the dye and spiro-MeOTAD L_{abs}, which was calculated by formula (1). Dividing the IPCT values, represented by the points 4, the values 5 of APCE were calculated.

Some characteristic features of the APCE spectra can be seen in Figure 3.21. The APCE values at the long wave end of the spectrum are low. This means that the dye molecules, excited into the energetic level just above the LUMO, possess only small probability to create free charge carriers capable to make input into the SC performance. About 0.3 eV more energy is needed to reach the APCE maximum. This is to be considered while tuning the energy levels in the SC. The electrons from the excited dye molecules need to be injected into the conduction band of TiO_2, the bottom of which is about 4.1 eV. The holes should jump into the HOMO level of the hole transporting material, which is at 5.0 eV. We see from Table 2 that the EA values for the dyes on TiO_2 are above 3.2 eV for the non-aggregated molecules and above 3.7 eV for the aggregates. Thus, there should be no problem for electrons to be injected into TiO_2, even from aggregates. Similarly, the I_p

values of the investigated dyes on TiO_2 are below 5.06 eV. Thus, there also should be no problem with the hole injection from the dye into the transporting material. However the steep IPCE dependence on the excitation quanta energy at the low energy side suggests that there is some mechanism influencing the injection efficiency. Probably molecular vibrations stimulate the charge carrier injection either into TiO_2 or into the transporting layer, or into both.

After reaching the maximum the APCE values decrease with further increase of the exciting light energy. This results in a bend in the APCE spectrum and corresponds to the maximum in the light absorbance spectrum. It may be caused by a lower efficiency of the charge carrier pairs generated near the FTO layer as compared with the pairs generated near to the spiro-MeOTAD layer due to the difficulty for holes to escape from the deep regions of the nanoporous TiO_2 layer. At wavelengths below 450 nm the APCE values once more decrease, this time because of the non-productive light absorption by the doped spiro-MeOTAD.

3.3.3. Summary of dyes investigation

The results of these investigations show that both the HOMO and LUMO values of the dyes used in SC are dependent on the aggregate state of the dyes. Energy levels differ quite noticeably depending upon the measurement conditions. For this reason the ionization potential and electron affinity of the dyes adsorbed on nanoporous TiO_2 should be evaluated. From the standpoint of the structure/energy level relationship it is evident that long aliphatic chains, positioned at π-conjugated bridges or the donor end of the molecule, inhibit formation of aggregates to some extent. This makes energy levels more predictable and closer related to the molecular structure. The results of this work also show that the absorbed photon conversion-to-current efficiency depends on the energy of the exciting light quanta. The maximum efficiency is reached when the quanta energy exceeds the threshold value by about 0.3 eV, which may be caused by some peculiarities of the charge carrier injection from the excited dye into TiO_2 or hole transporting material.

4. Conclusions

- In order to proper determine energetic levels of dyes, used in DSSCs, especially HOMO level, all measurements should be carried on dyes, adsorbed on TiO_2 layer, thus taking into consideration impact of interaction between dyes and TiO_2 also.
- Investigated carbazole-based diamine V997 has good charge transporting properties, it has energetic levels compatible to the perovskite levels, thus it does not make any barrier for charge carriers from the perovskite into V997. This lets to work as efficiently as Spiro-OMeTAD in perovskite Solar cells. With consideration of cheaper synthesis, investigated diamine is effective replacement of Spiro-OMeTAD.
- With taking into account a relationship between structure of dyes and its energetic levels, we can see that long aliphatic groups reduces a formation of aggregates, if those groups are attached to the π-conjugated bridges or donors.
- In these investigations we have found also, that absorbed photon-to-current conversion efficiency (APCE) is dependable on initiated quanta energy, and the maximum point is reached, when energy of quanta exceeds 0.3 eV threshold value.
- In investigated phenothiasine-based hydrazones the replacement of methyl- groups with phenyl- groups does not affect ionization potential nor hole mobility.
- Introduction of additional aromatic groups in carbazole-based hydrazones increases hole mobility 4-30 times, and affects ionization potential by 0.04-0.07eV also.

5. Bibliography

[1] B. O'Regan, M. Grätzel, Low-cost, high-efficiency solar cell based on dye-sensitized colloidal tio2 films, Nature **353**, 737–740 (1991).

[2] M. Grätzel, Photoelectrochemical cells, Nature **414**, 338–344 (2001).

[3] M. K. Nazeeruddin, F. De Angelis, S. Fantacci, G. Selloni, A.and Viscardi, P. Liska, T. Ito, S.and Bessho, M. Grätzel, Combined experimental and dft-tddft computational study of photoelectrochemical cell ruthenium sensitizers, J. Am. Chem. Soc. **127**, 16835–16840 (2005).

[4] Y. Chiba, A. Islam, Y. Watanabe, R. Komiya, N. Koide, L. Y. Han, Dye-sensitized solar cells with conversion efficiency of 11.1**45**, L638–L640 (2006).

[5] F. Gao, Y. Wang, D. Shi, J. Zhang, M. K. Wang, X. Y. Jing, R. Humphry-Baker, P. Wang, S. M. Zakeeruddin, M. Grätzel, Enhance the optical absorptivity of nanocrystalline tio2 film with high molar extinction coefficient ruthenium sensitizers for high performance dye-sensitized solar cells, J. Am. Chem. Soc. **130**, 10720–10728 (2008).

[6] Y. M. Cao, Y. Bai, Q. J. Yu, Y. M. Cheng, S. Liu, D. Shi, F. Gao, P. Wang, Dye-sensitized solar cells with a high absorptivity ruthenium sensitizer featuring a 2-(hexylthio)thiophene conjugated bipyridine, J. Phys. Chem. C. **113**, 6290–6297 (2009).

[7] C. Y. Chen, M. K. Wang, J.-Y. Li, N. Pootrakulchote, L. Alibabaei, C. H. Ngoc-le, J. D. Decoppet, J. H. Tsai, C. Grätzel, C. G. Wu, et al, Highly efficient light-harvesting ruthenium sensitizer for thin-film dye-sensitized solar cells, ACS Nano **3**, 3103–3109 (2009).

[8] A. Yella, H.-W. Lee, H. N. Tsao, C. Yi, A. K. Chandiran, M. Nazeeruddin, E. W.-G. Diau, C.-Y. Yeh, S. M. Zakeeruddin, M. Grätzel, Porphyrin-sensitized solar cells with cobalt (ii/iii)–based redox electrolyte exceed 12 percent efficiency, Science **334**, 629–634 (2011).

[9] S. Kim, J. K. Lee, S. O. Kang, J. Ko, J.-H. Yum, S. Fantacci, F. De Angelis, D. Di Censo, M. K. Nazeeruddin, M. Grätzel, Molecular engineering of organic sensitizers for solar cell applications, J. Am. Chem. Soc. **128**, 16701–16707 (2006).

[10] D. P. Hagberg, T. Edvinsson, T. Marinado, G. Boschloo, A. Hagfeldt, L. C. Sun, A novel organic chromophore for dye-sensitized nanostructured solar cells, Chem. Commun. 2245–2247 (2006).

[11] W. D. Zeng, Y. M. Cao, Y. Bai, Y. H. Wang, Y. S. Shi, M. Zhang, F. F. Wang, C. Y. Pan, P. Wang, Efficient dye-sensitized solar cells with an organic photosensitizer featuring orderly conjugated ethylenedioxythiophene and dithienosilole blocks, Chem. Mater. **22**, 1915–1925 (2010).

[12] N. Cai, S.-J. Moon, L. Cevey-Ha, T. Moehl, R. Humphry-Baker, P. Wang, S. M. Zakeeruddin, M. Grätzel, An organic d-π-a dye for record efficiency solid-state sensitized heterojunction solar cells, Nano Lett. **11**, 1452–1456 (2011).

[13] X. Liu, W. Zhang, S. Uchida, L. Cai, B. Liu, S. Ramakrishna, An efficient organic-dye-sensitized solar cell with in situ polymerized poly(3,4-ethylenedioxythiophene) as a hole-transporting material, Adv. Mater. **22**, E150–E155 (2010).

[14] A. Snaith, H. J. Petrozza, S. Ito, H. Miura, M. Grätzel, Charge generation and photovoltaic operation of solid-state dye-sensitized solar cells incorporating a high extinction coefficient indolene-based sensitizer, Adv. Funct. Mater. **19**, 1810–1818 (2009).

[15] Y. Wu, W.-H. Zhu, S. M. Zakeeruddin, M. Grätzel, Insight into d-a-π-a structured sensitizers: A promising route to highly efficient and stable dye-sensitized solar cells., ACS Appl. Mater. Interfaces **7**, 9307–9318 (2015).

[16] M. Daskeviciene, V. Getautis, J. V. Grazulevicius, A. Stanisauskaite, J. Antulis, V. Gaidelis, V. Jankauskas, J. Sidaravicius, Crosslinkable carbazolyl-containing molecular glasses for electrophotography, The Journal of Imaging Science and Technology **5**, 467–472 (2002).

[17] S. Urnikaite, T. Malinauskas, V. Gaidelis, I. Bruder, R. Send, R. Sens, V. Getautis, Simple and inexpensive organic dyes with hydrazone moety as π-conjugated bridge for solid-state dye-sensitized solar cells, Chem. Asian J. **8**, 538–541 (2013).

[18] S. Urnikaite, T. Malinauskas, V. Gaidelis, I. Bruder, R. Send, R. Sens, V. Getautis, Organic dyes with hydrazone moeties: A study of correlation between structure and

performance in the solid-state dye-sensitized solar cells, J. Phys. Chem. C **118**, 7832–7843 (2014).

[19] S. Urnikaite, M. Daskeviciene, R. Send, H. Wonneberger, A. Sackus, I. Bruder, V. Getautis, Organic dyes containing a hydrazone moiety as auxiliary donor for solid-state dssc applications, Dyes and Pigments **114**, 175–183 (2015).

[20] N. G. Connelly, W. E. Geiger, Chemical redox agents for organometallic chemistry, Chem. Rev. **96**, 877–910 (1996).

[21] Zoski, G. Cynthia, ed., *Handbook of electrochemistry* (Elsevier, 2006).

[22] B. Peng, G. Jungmann, C. Jager, D. Haarer, H. W. Schmidt, M. Thelakkat, Systematic investigation of the role of compact tio2 layer in solid state dye-sensitized tio2 solar cells, Coord. Chem. Rev. **248**, 1479–1489 (2004).

[23] H. Bässler, Charge transport in disordered organic photoconductors a Monte Carlo simulation study, physica status solidi (b) **175**(1), 15–56 (1993).

[24] Y. Hua, B. Xu, P. Liu, H. Chen, H. Tian, M. Cheng, L. Kloo, L. Sun, High conductivity Ag-based metal organic complexes as dopant-free hole-transport materials for perovskite solar cells with high fill factors, Chem. Sci. **7**(4), 2633–2638 (2016).

[25] W. H. Nguyen, C. D. Bailie, E. L. Unger, M. D. McGehee, Enhancing the Hole-Conductivity of Spiro-OMeTAD without Oxygen or Lithium Salts by Using Spiro(TFSI) $_2$ in Perovskite and Dye-Sensitized Solar Cells, Journal of the American Chemical Society **136**(31), 10996–11001 (2014).

[26] A. Heckmann, C. Lambert, Organic Mixed-Valence Compounds: A Playground for Electrons and Holes, Angewandte Chemie International Edition **51**(2), 326–392 (2012).

[27] M. L. Petrus, T. Bein, T. J. Dingemans, P. Docampo, A low cost azomethine-based hole transporting material for perovskite photovoltaics, J. Mater. Chem. A **3**(23), 12159–12162 (2015).

A. Absorption, IPCE, APCE spectra for dyes D1-D9

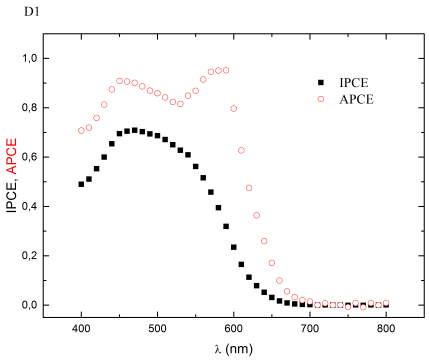

(a) APCE and IPCE of dye D1

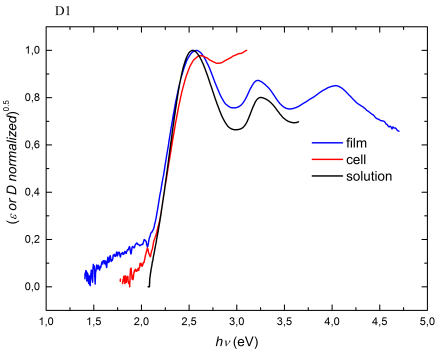

(b) Absorbance spectra of dye D1

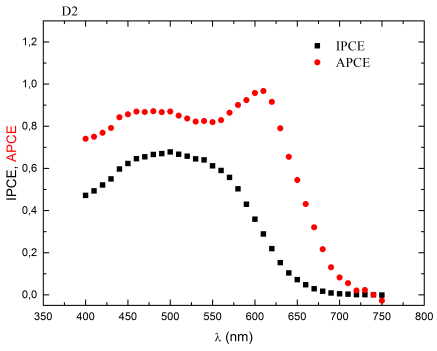

(a) APCE and IPCE of dye D2

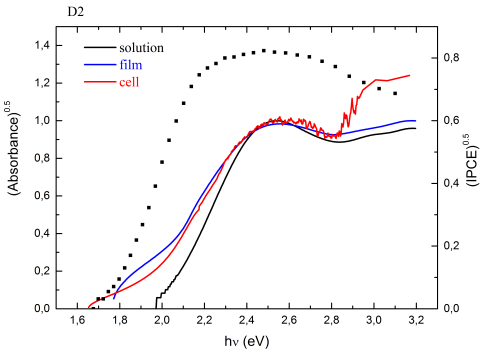

(b) Absorbance and IPCE of dye D2

A. Absorption, IPCE, APCE spectra for dyes D1-D9

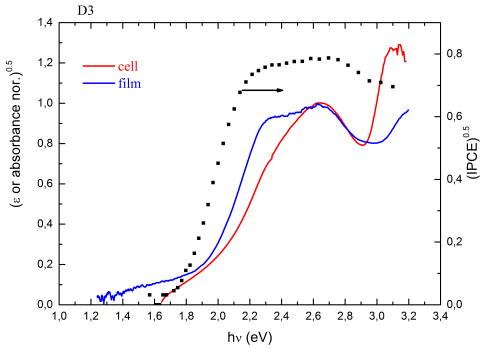

(a) Absorbance and IPCE of dye D3

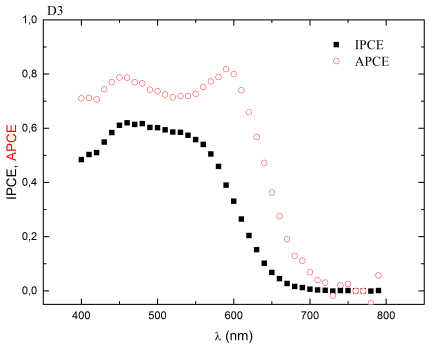

(b) APCE and IPCE of dye D3

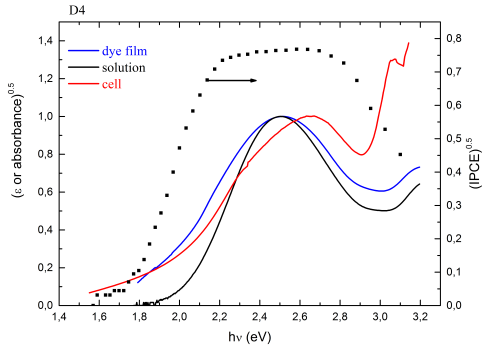

(a) Absorbance and IPCE of dye D4

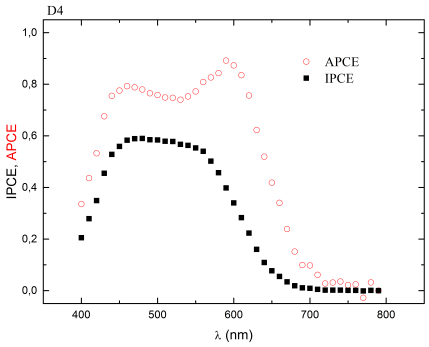

(b) APCE and IPCE of dye D4

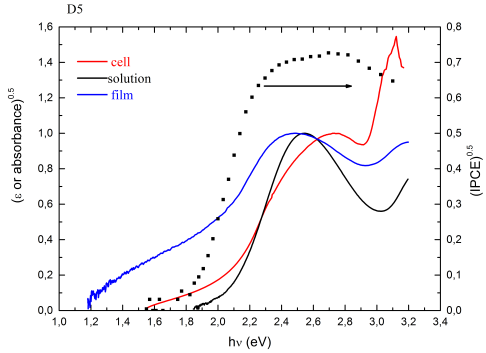

(a) Absorbance and IPCE of dye D5

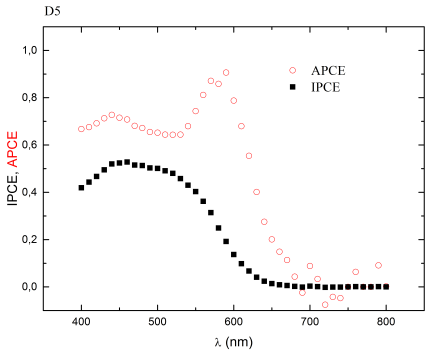

(b) APCE and IPCE of dye D5

A. Absorption, IPCE, APCE spectra for dyes D1-D9

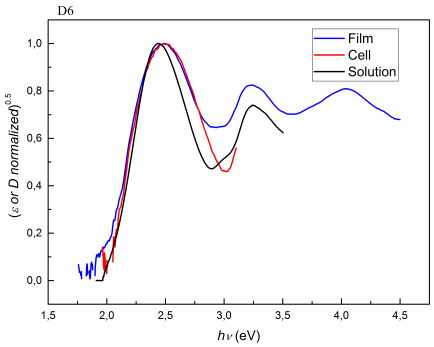

(a) Absorbance spectra of dye D6

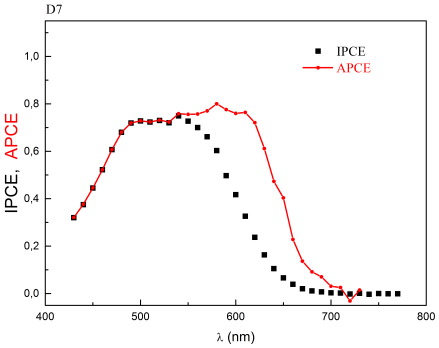

(b) APCE and IPCE of dye D7

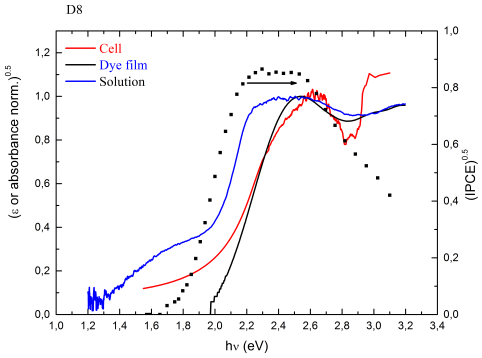

(a) Absorbance and IPCE of dye D8

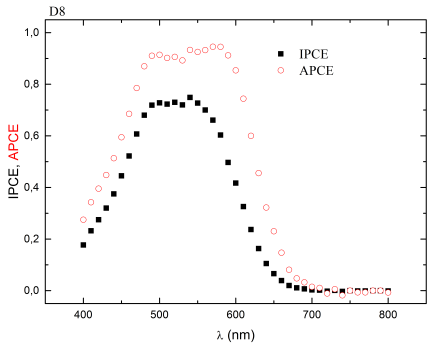

(b) APCE and IPCE of dye D8

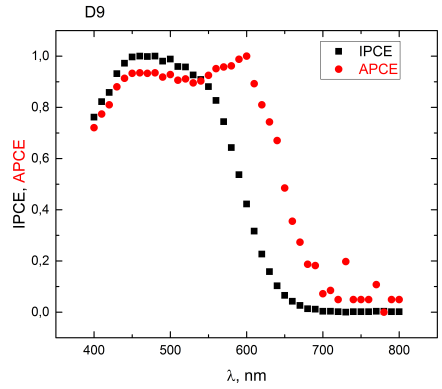

(a) APCE and IPCE of dye D9

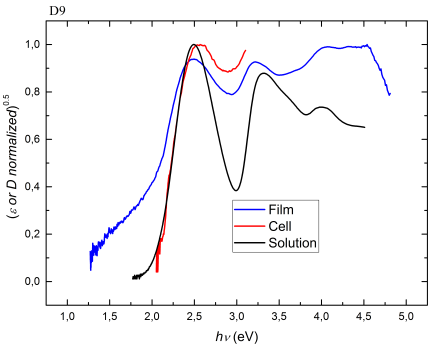

(b) Absorbance spectra of dye D9

B. Kinetics of small charge in hole-transporting materials in differential mode

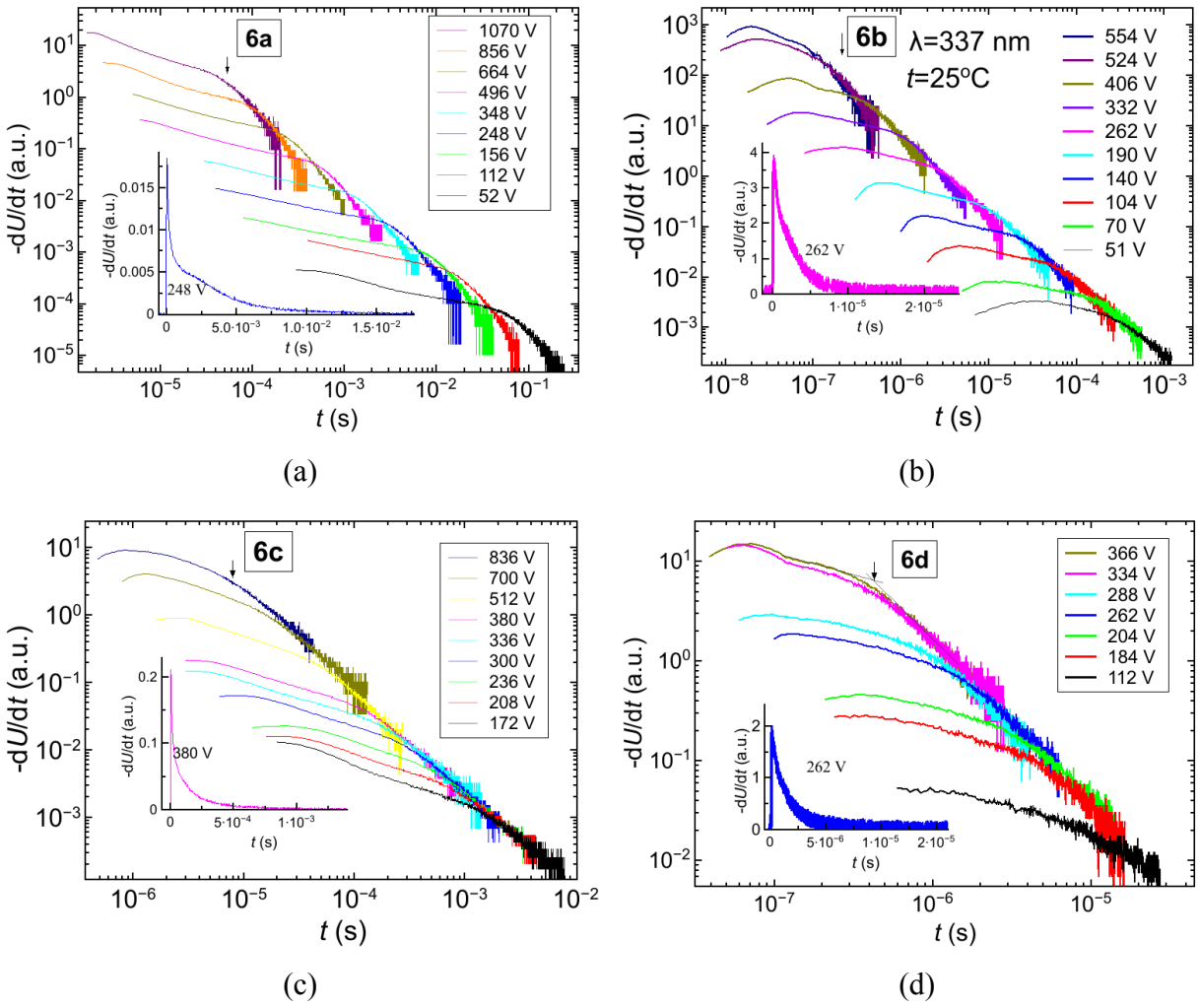

Figure S1.: Kinetics in a) - **6a**, b) - **6b**, c) - **6c**, d) - **6d**

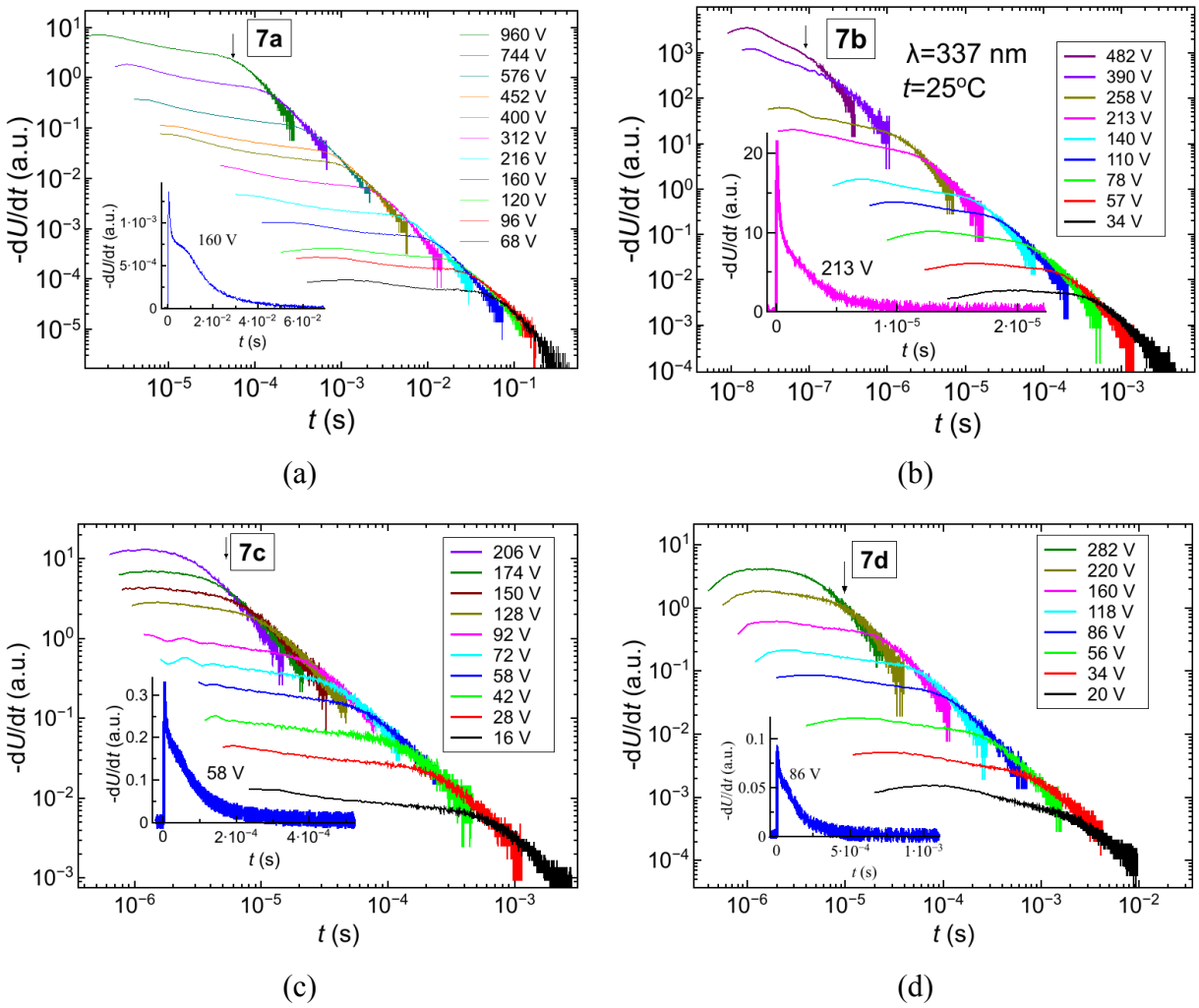

Figure S2.: Kinetics in a) - **7a**, b) - **7b**, c) - **7c**, d) - **7d**

C. Kinetics of small charge in hole-transporting materials in integral mode

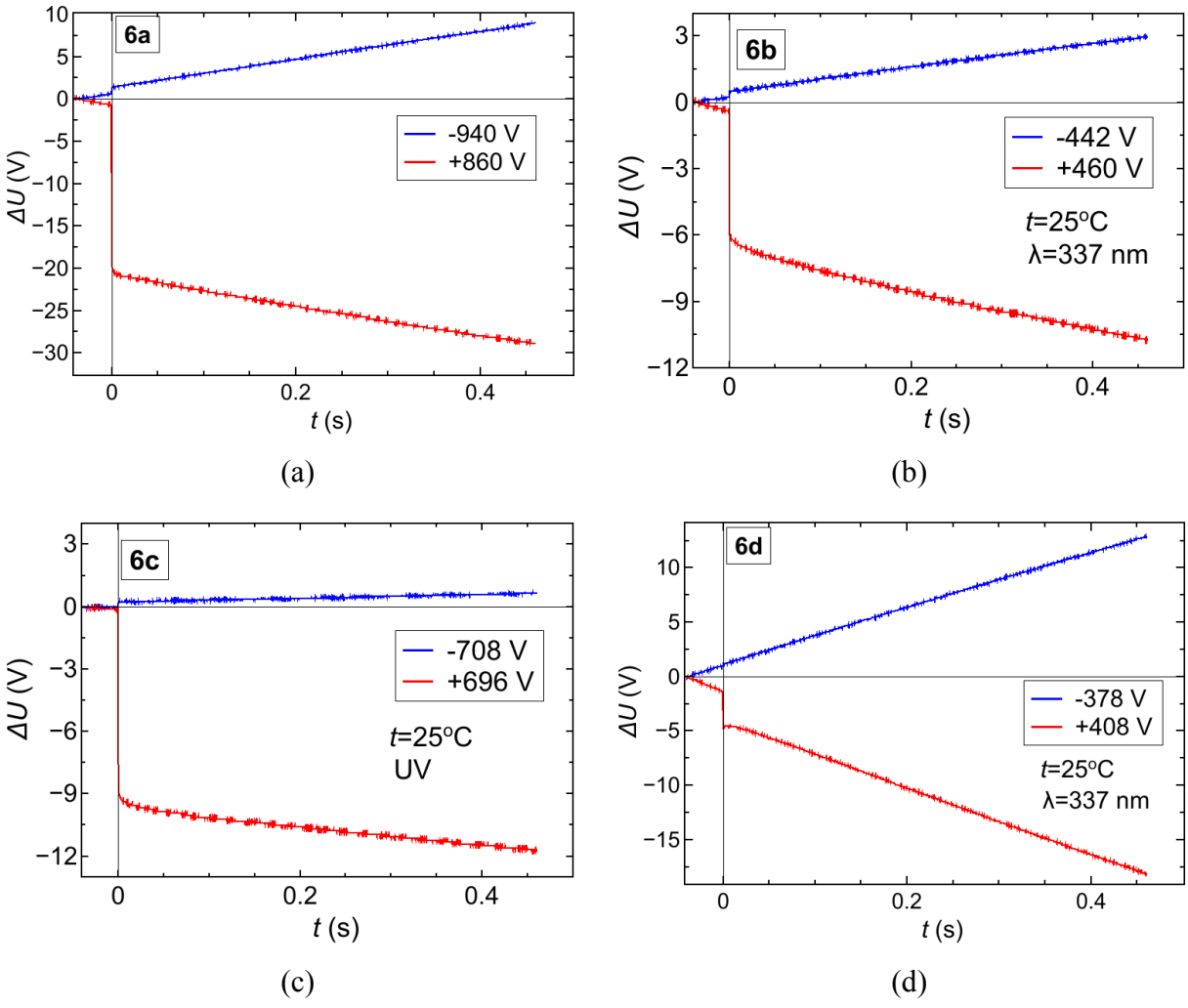

Figure S1.: Kinetics in a) **6a**, b) **6b**, c) **6c**, d) **6d** materials.

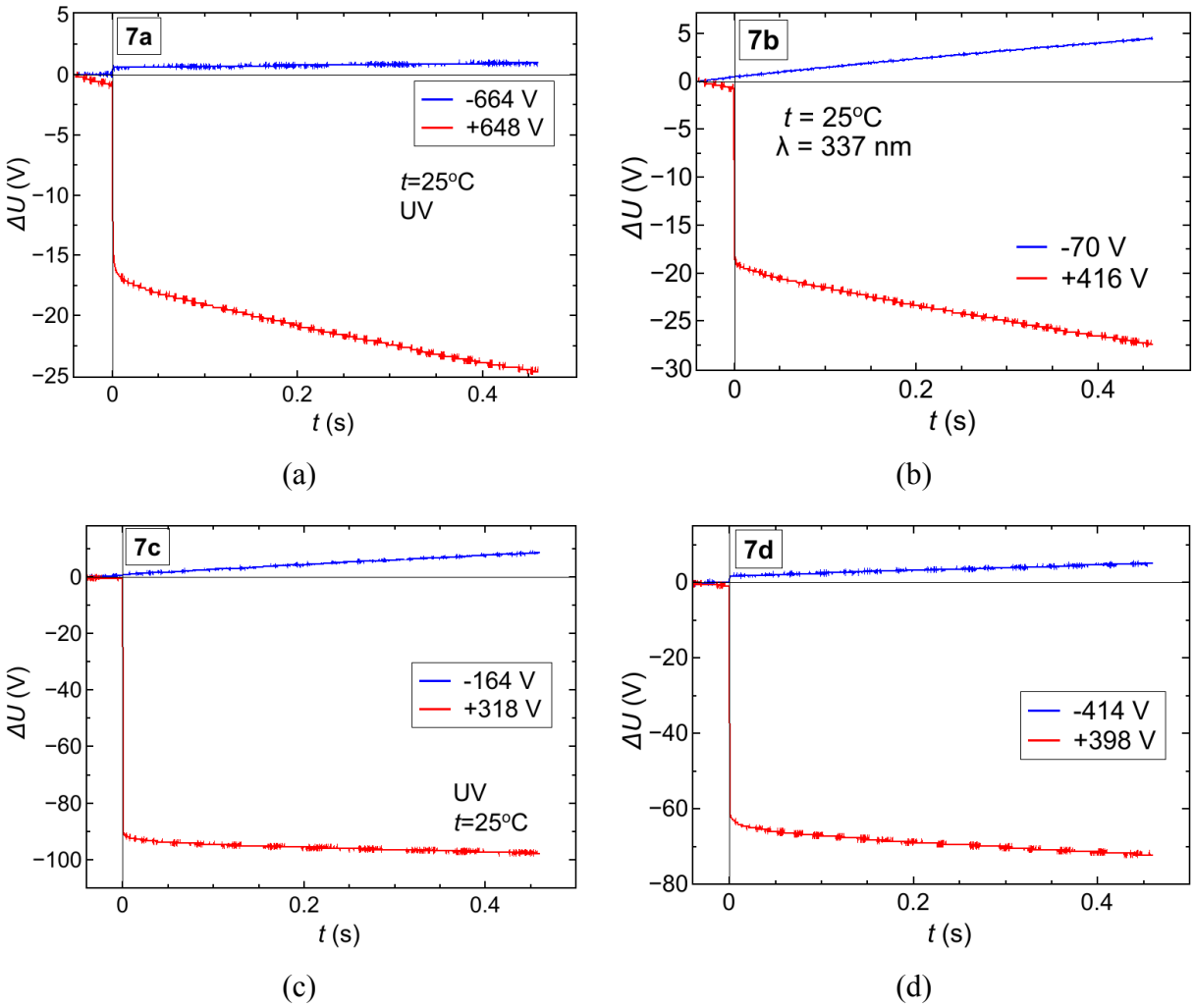

Figure S2.: Kinetics in: a) **7a**, b) **7b**, c) **7c**, d) **7d** materials.

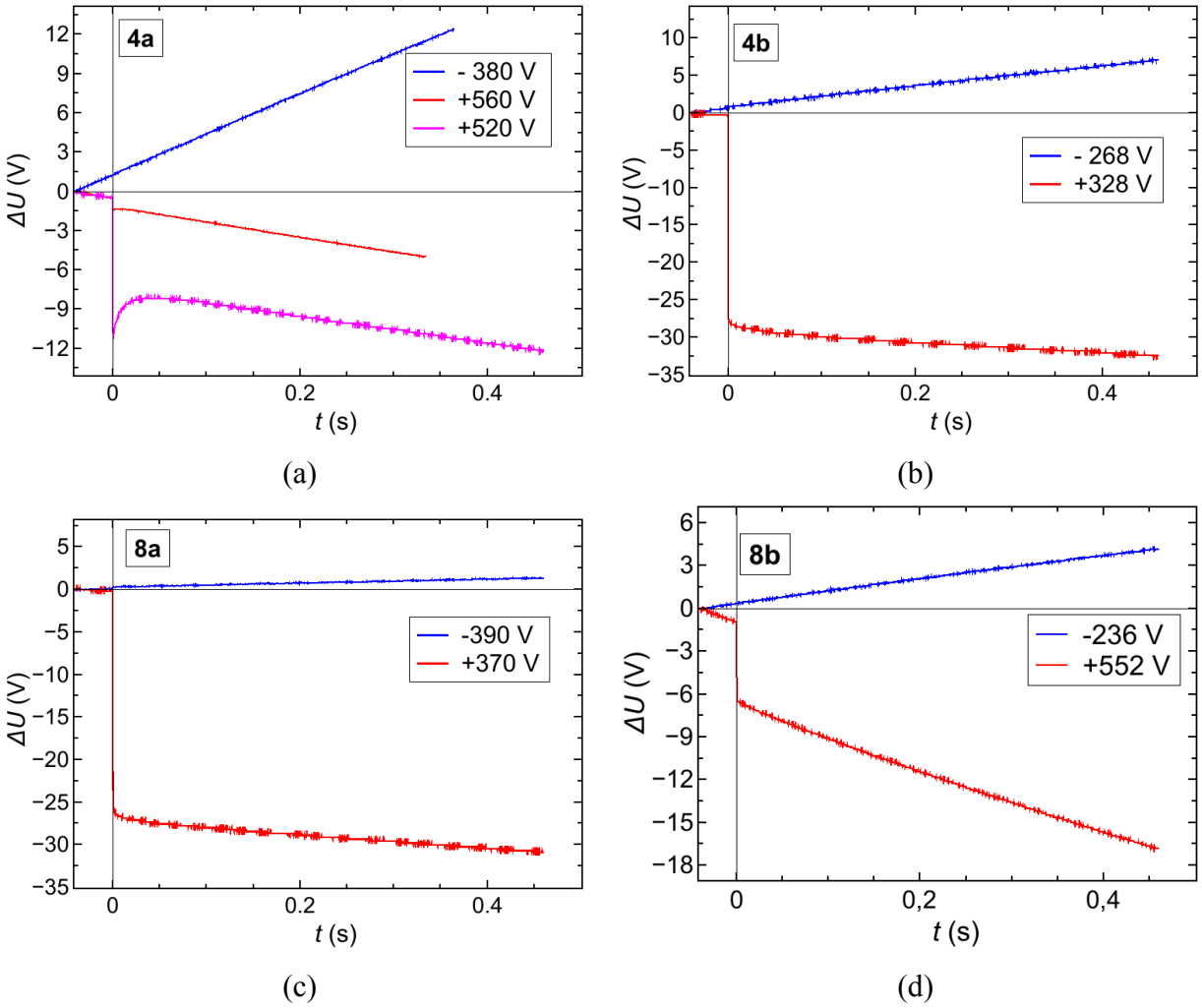

Figure S3.: Kinetics in: a) **4a**, b) **4b**, c) **8a**, d) **8b** materials.

CV

Egidijus Kamarauskas

Saulėtekio 41 - 118
Vilnius, LT-10223
+370 607 07356
egidijus.kamarauskas@gmail.com

EDUCATION

Bachelor degree in electronics engineering,
Vilnius university, 2008
Master degree in material science
Vilnius university, 2010
PhD studies ,
Vilnius university, 2010 - present

SOFTWARE

Programming languages and applications: MS Office, LibreOffice, Microcal Origin, MATLAB, AutoCAD, Bash, FreePascal, LaTeX, Python (PyQt4), C/C++ (basics), C# (basics).
Operating systems: Windows, Linux (Ubuntu, SLED).

EXPERIENCE

Technician 2003 - 2004
UAB „Enigmalita“
- Control of SMD assembly line, quality control.

Physics teacher 2010
Vilnius youth school of J. Ivaškevičius
- Physics teaching.

Engineer 2008 - 2016
Vilnius university

Junior researcher 2013-present
Vilnius university